POLITECNICO DI TORINO

Corso di Laurea Magistrale in Ingegneria Aerospaziale

TESI DI LAUREA MAGISTRALE

Experimental Study of a Resonance Igniter for Rocket Engines

Relatore

Prof. Dario Pastrone

Co-relatori

Ing. Andrea Ferrero

Ing. Filippo Masseni

Candidato

Giulio Panzarasa

Anno Accademico 2020/2021

……. A volte i sogni

si realizzano …….

Dedico questa tesi ai miei genitori

che mi hanno sostenuto durante

la mia carriera scolastica e universitaria

permettendomi di raggiungere questo importante traguardo

Abstract

Nowadays, one of the most widely used propellants for aerospace propulsion are based on hydrazine derivates which can be easily ignited due to the hypergolic properties of hydrazine/nitrogen tetroxide combinations. It is well known that this fuel has been used for a long time and it has contributed to the creation of ad-hoc and very reliable propulsion systems. However, there are some problems related to its polluting and toxic effects, which are no longer tolerated in today's society. These aspects have led the researchers to focus on less polluting propellants which, unfortunately, do not have hypergolic properties thus requiring more efforts in the development of new ignition systems, such as the resonance-based ignition system.

This device uses the energy of the propellant itself in the form of pressure to cause ignition through a so-called resonant igniter, which has many advantages like the lack of both moving parts and electrical circuits.

The aim of this thesis is to carry out an experimental and comprehensive investigation of the ignition method. After a first part of the work dedicated to the analysis of the historical development and the state of the art, the experimental section follows. This experimental part contains the description of the tests performed, the modifications applied to the experimental apparatus and the different geometries of the resonator. The latter is the main component of the ignition system, whose shape greatly influences the outcome of the experiments.

In the final part, we collected the results emerged during the study including the indication of the maximum temperatures reached in the tests that in some configuration exceeded 1000 K. The results obtained are in line with the findings of other research groups and represent a solid background for further studies.

Contents

Chapter 4: Conclusions

List of Figures

List of Tables

Chapter 1

Introduction and Historical Notes

In this first chapter, consisting of two sections, a first description of the phenomenon will be provided. The introductory part describes the current situation, the attention to the environment and the main components of the resonance system; follows by an historical section where the events, that have seen this system as a protagonist, are retraced, from 1919 to the present day.

1.1 Introduction

The first references to the concept of resonance date back to 1919 with Hartmann's experiments. As we will see in the historical chapter, he was not interested in the thermal aspects, which were still undiscovered at that time, but in the sound source.

We need to wait until 1954 when Sprenger focuses on the thermal effects related to the resonance phenomenon.

Starting from the first discoveries numerous steps forward and improvements have been taken to the present day.

Nowadays hydrazine is widely used for thrusters during orbital maneuvers because it is storable and when used in combination with N_2O_4 a hypergolic mixture is obtained; this led to the development of the combustion systems and related components in depth, contributing to the definition of the reliability of all systems that apply this fuel.

The important efforts towards lower environmental impact and reduced emissions have brought out some problems related to hydrazine i.e. its ecological hazard due to its deep toxicity. In fact in Europe, hydrazine is classified as a dangerous propellant and therefore a new interest has emerged in the research of less polluting alternative propellants, for example the liquid Oxygen/liquid Methane (LOX / LCH_4) mixture which however does not have the hypergolic property of monomethylhydrazine, [5] consequently an ignition system need to be employed.

The characteristics of the resonance ignition system are of considerable interest and insist on the creation of a light, reliable and passive device able to operate for a high number of cycles and with a long duration without requiring an electrical

system for ignition, [3] thus overcoming some problems of previous systems such as wiring insulation, complexity and high frequency electrical interference.[1]

After the description of the characteristics, we can briefly list the possible applications of this system: first of all the application for the rocket engine, for the removal of debris in orbit where numerous engine restart process are required [5] but also for acoustic damping, passive preheater of the propellant for scramjet [3] and emergency system for the crew. Since the resonance phenomenon is also known for the sound effect, these high intensity waves can be used for fog dissipators [6] or as actuators.[10]

The system is mainly based on a nozzle, that generates an under-expanded flow, and a tube named resonator, with a closed cavity of various geometries. The resonator inlet faces the nozzle exit, while being mounted coaxially. The diameter of the resonator cavity is generally greater than that of the nozzle outlet. [14]

After this premise, in the following parts different resonator geometries will be analysed. During the tests, the effects of the variation of some parameters and the maximum achievable performances in terms of temperature will be reported, in the resonance igniter system in fact the key point is the heating process of a small part of gas capable to determine the phenomenon of combustion.

1.2 Historical Notes: from the Origins to the Present Day

In the available literature, the first references to resonance phenomenon are dated back to 1919 with Hartmann's studies, which focused on the sound effects produced by exploiting resonance phenomenon.[1] During the first experiment in 1922, two shapes were used for the cavity: a bulb and a cylindrical one involving air and hydrogen as gas. Due to the generated phenomena, the latter type of cavity is called resonator.[7] The initial test setup included a converging nozzle and a closed cavity at one end through which flows an under-expanded jet producing an intense high frequency noise.[3] For this reason, the device was initially called "Hartmann whistle". [10]

In the series of experiments that followed from 1919 to 1951 Hartmann tested different geometries of nozzle and cavity, observing the effects caused by the variation of the distance between nozzle and resonator as reported in his 1939 publication and in the 1927 study of Hartmann and Trolle, where it was suggested a resonator length of 1-2 times the diameter.[10] It is therefore possible to understand from these initial tests dating at the beginning of the 1900s, that the

nozzle-resonator distance plays an important role, thus becoming one of the main parameters to be considered during the tests.

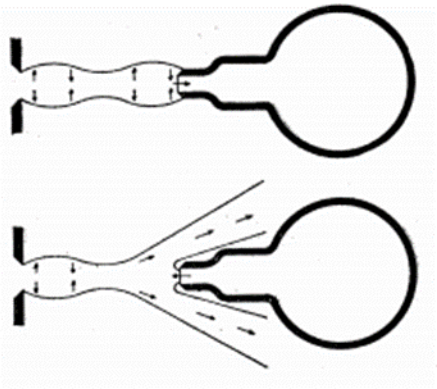

Figure 1.1: Bulb shape used in early Hartmann's experiments of 1922 [7]

Sprenger, Thompson and Kang considered instead the resonator as a way to obtain high temperature gases.[1] Sprenger studied the effects of intense heating process near the closed end of the resonator. The scientist attributed these effects to shock waves that repeatedly compressed the gas inside the cavity [3] and in 1954 he began to study the variations of the maximum temperature obtainable at the end of the resonator by editing some parameters such as the nozzle-cavity distance and the resonator length.[6] A classification of these variables can be found in Phillips and Pavli's article of 1971.

The first experiments carried out did not lead to a large increasing in temperature, this is because the correct criteria were not applied, for example the resonator walls were too thicker, in fact Hartmann detected an increase of only 7 °C; Sprenger was the first to detect significant increase in temperature reaching 425 °C with an air-powered resonator.[10]

Other experiments followed like the ones carried on by Hall and Berry in 1959, during which they detected a temperature increase of 140 °C with a gas at stagnation temperature of 20 °C.[10]

In the following years resonance effect have been studied with growing attention by many researchers, either from the point of view of sound generation waves and from the thermal one. It is therefore necessary to make a distinction between "Powered Resonance Tube" (PRT), related to noise emissions, and "Hartmann-Sprenger Tube" (HST) if we are interested in thermal phenomena. We can find an

example of PRT studies in Raman and Kibens experiments, which demonstrated the application of this system to control flow.[10]

With particular reference to HST, Sarohia and Bach identified three different resonator operating modes:[9]

- jet instability mode (JIM)

- jet regurgitant mode (JRM)

- jet screech mode (JSM)

During their experiment that took place in 1979, it emerged that heating is linked to the operating mode. In particular in the screech mode the temperature reached is higher than the regurgitant mode ones.[10]

It was shown that for different types of resonators, a rapid heating of the gas near the bottom cavity could be obtained.[12] The causes of this heating are mostly due to dissipative processes such as the increase in entropy through compression waves [12] and wall friction as reported by Kawahashi.[10]

Differences were found in the increase of the equilibrium temperature between monoatomic and bi-atomic gases, in particular the former provided higher temperatures.[16]

In the first phase of the cycle, the inflow phase, compression waves move within the cavity and their intensity and strength increases with the increasing length of the cavity itself.[12]

Regarding the research for dissipative sources, Brocher and Maresca reported that the most influential mechanism is mass exchange which removes generated heat in the resonator. This exchange takes place between the flow coming from the nozzle and the hot one of the resonator,[10] this is definitely a limitation on the maximum achievable temperature in the Jet Regurgitant mode.

After this first historical parenthesis, we reached the first tests of the system considering its possible application such as the 1967 studies by Conrad and Pavli aimed at demonstrating the application of the Hartmann-Sprenger resonator for the ignition of rocket engines powered by hydrogen and oxygen.[3]

At the same time, greater attention was focused on geometric details: in 1970 McAlevy and Pavlak used traditional and conical cavities to better understand resonance phenomenon, reiterating the importance of the section near the cavity entrance.[10]

Changes were also made to the nozzle. Initially the resonance phenomenon was considered possible only in supersonic condition, but the studies carried out by

Savory, Hartmann and Trusdo showed that pressure oscillations also occurred in subsonic condition using a nozzle with an axial stem.[10]

Neemeh in 1984 and Rakowsky in 1974 analysed the thermal effects related to conical cavities while Brocher and Kawahashi studied resonators with stepped geometry, they observed a greater heating in the resonator with sinusoidal transition.[10]

In 1983 also Brocher and Ardisssone carried out experiments on the effects of various parameters, such as material and type of gas. They used a resonator with stepped structure and they compared its performance with the classic cylindrical shape. The performance obtained with the stepped cavity resulted better, almost comparable to the conical one,[8] furthermore the use of a material with low thermal conductivity led to higher temperatures. Finally, with the application of a needle protruding from the nozzle, temperature increase was recorded at the end of the wall.[10]

On the other end, the conical cavity still performs better as demonstrated by Rakowsky in 1974 and Kawahashi in 1984, who observed a greater heating of the resonator.[12]

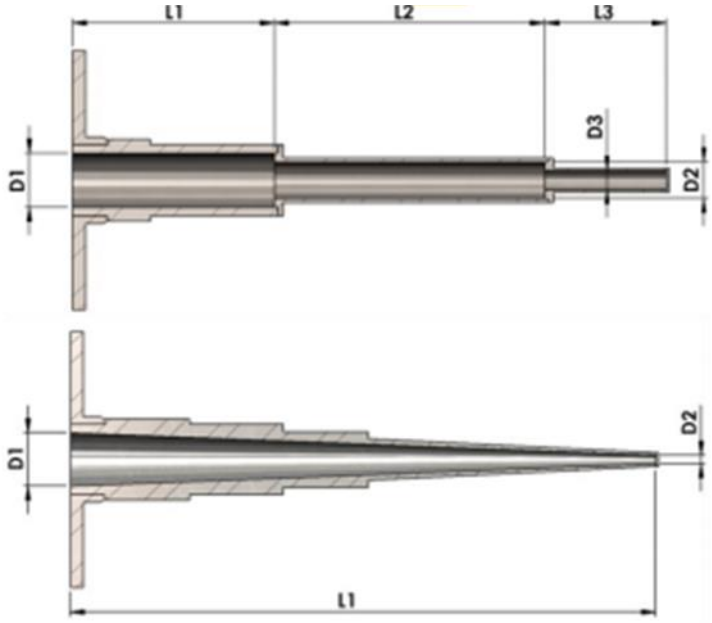

Figure 1.2: Resonator shapes, stepped shape at the top, conical cavity at the bottom. As described, the characteristics of the first are almost comparable with the latter ones [3]

Comparing the resonance frequencies, Sreejith and colleagues noted lower values for the cylindrical resonator compared to the one with conical cavity.[11] Regarding frequency studies, Kawahashi and colleagues were the first in 1983 to relate the variation of frequency oscillations with geometric parameters such as

the ratio between diameters for a stepped cavity and the ratio between the lengths of its two segments for a system subjected to sonic flow.[15]

In the analysis of operational stability during ignition, the response time represented a unit measure and the temperature variation inside the resonator is the reference for its calculation. In particular Marchese and colleagues reported higher values of response time for stepped geometry compared to the cylindrical one and an intermediate value for the conical cavity.[16]

According to Iwamoto in 1990, the presence of a low-pressure region on the external surface of the resonator walls and a positive gradient near the opening of the same are the necessary conditions to create and maintain an efficient resonance inside the Hartmann-Sprenger tube.[12]

In 1991 Sobieraj and Szumowski analysed various configurations of the mechanism, such as the combination of two resonators and a single flow. They also reported that the shape of inlet cavity has remarkable thermal and sound effects while the nozzle's outlet shape is negligible.[10]

Later, Kastner and Samimy carried out studies on the effects of the resonator length, specifically they noticed that the amplitude corresponding to the fundamental frequency decreases with the increasing of the cavity length.[10]

In the 2000s numerical analysis techniques have been developed: Chang and Lee studied the JRM mode inside the resonator with the Euler equations, they presented a simplified model to numerically simulate the internal flow process.[14] Hammed and collaborators applied the Navier-Stokes equations for compressible and viscous flow, while Murugappan and Gutmark the Fluent software with an implicit first-order scheme.[11]

At the end of this historical overview, it is necessary to mention some "non-propulsive" developments aimed at demonstrating possible applications in addition to the aforementioned ignition system for rocket engine.

Regarding to sound waves emissions, we can focus the attention on the studies by Brun and Brocher of 1957, in which they have used the resonator for the dissipation of fog by generating high intensity ultrasonic waves.[12]

Later, in 1975 Brocher and Betton proposed a resonant system able to convert heat into electrical energy.[10] In the same year, Merkli and Thomann showed that cooling was also possible with the use of the resonance tube. In this context, a first analytical study has provided for the energy transport process explaining the distribution of heat flux inside the cavity,[13] also Kadaba in 1990 applied this mechanism to the refrigeration system,[10] while Kawahashi, Suzuki, Arkharov and Bondarenko investigated the use of the Hartmann-Sprenger tube as a replacement for the expansion valve in cryogenic and refrigerant applications.[16]

To conclude, Kastner and Samimy in 2002 has developed a fluidic actuator with Hartmann's resonator [12] and, in 2003 Bouch and Cutler applied the Hartmann-Sprenger resonant tube to the operating cycle of a scramjet.[10]

Chapter 2

Resonance Effect and Operation Modes

In this second chapter the resonance phenomenon will be analyzed in detail; in fact in the first section, the functioning of the resonator is shown, followed by a second part in which the three particular modes of operation are described. To conclude, a section concerning the parameters that affect the operation and performance of the resonator is reported.

2.1 Operation

Many attempts have been made in order to explain the phenomenon of resonance, starting from Hartmann himself in the 1920s coming to Smith and Powell experiments with the introduction of the term "instability zone". This area is included in the structure formed from the pressurized flow leaving a sonic nozzle then discharging into the surrounding space in the status of under-expanded gas. As it is shown in *Figure 2.2*, these instability zones are characterized by a sudden increase in pressure and they are therefore compression zones.[10,14]

As soon as this jet hits a cavity, a detached shock will be formed in front of it remaining in a certain position as shown in *Figure 2.1.*[1] Due to the evaluation of the static pressure along the axis of the jet, it is possible to notice its oscillating aspect as shown in the second part of *Figure 2.2.*[10]

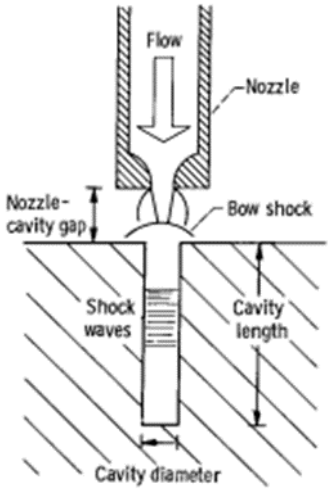

Figure 2.1: Simple description of the resonant system [1]

The modification of the motion field and the nozzle, if the cavity is placed inside these particular areas, will lead the detached shock to oscillate. These regions indicate the resonance conditions and correspond to the unstable areas shown in *Figure 2.2* where the pressure increase occurs.[1,10]

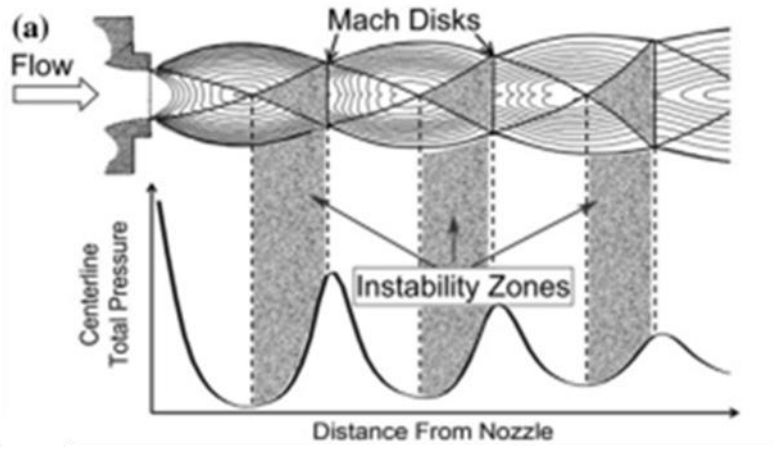

Figure 2.2: Under-expanded jet flow structure and instability zones [14]

Characteristically, in the tests carried out, the diameter of the cavity is slightly larger than the diameter of the nozzle [11] with the exception of the very first tests in which the diameters were approximately equal.

A description of the phenomenon was provided by Smith and Powell.

As mentioned above, it is necessary to arrange the resonator inlet within one of the instability areas.

In *Figure 2.3*, the flow directions are highlighted during the subsequent operating period, section A refers to the initial phase when the flow enters inside the resonator and the shock is very close to its inlet.[10] The compression waves detach from the curved oscillating shock present in front of the cavity inlet and enter in the resonator; after reaching the bottom, they are reflected to strengthen the external shock and join together, whereby as shown in *Figure 2.1*, there will be compression waves oscillating along the resonator cavity.[1] As filling proceeds, the pressure begins to gain and this action pushes the shock further upstream until it reaches a more stable position as shown in *Figure 2.3 B.*[10] There is therefore an increase in the temperature of the gas trapped near the closed end of the cavity as a result of the irreversible effects of collisions.[14]

A pressure decrease occurs at the entrance to the resonator cavity due to the displacement of the shock further upstream, expansion waves move towards the end wall and this causes the leakage of the flow contained in it. The latter will move radially outward causing a decrease in pressure behind the shock and its displacement downstream as indicated in *Figure 2.3 C* and *2.3 D.*[10]

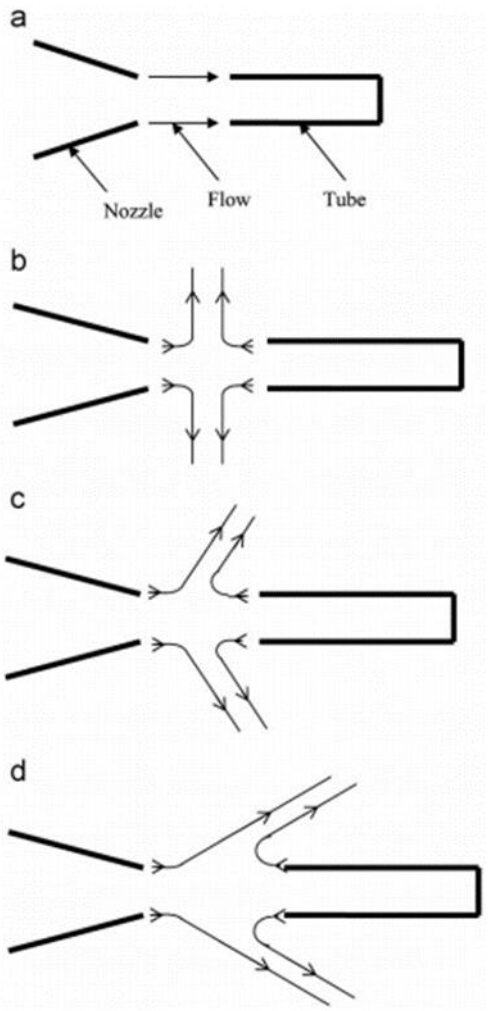

Figure 2.3: Description of the resonator operating phases [10]

After the pressure has returned to its initial value, the shock in front of the cavity and the expansion waves have reached the inlet of the cavity,[8] the filling phase begins again and the cycle ends.[10]

The various phases inside the resonator are summarized in the following *Figure 2.4*, there is also a dotted line that separates the area reached by the jet coming from the nozzle from that in which there is the trapped gas oscillating inside the resonator. In particular, if the Mach number increases, also the propagation length of the flow coming from the nozzle increases.[8]

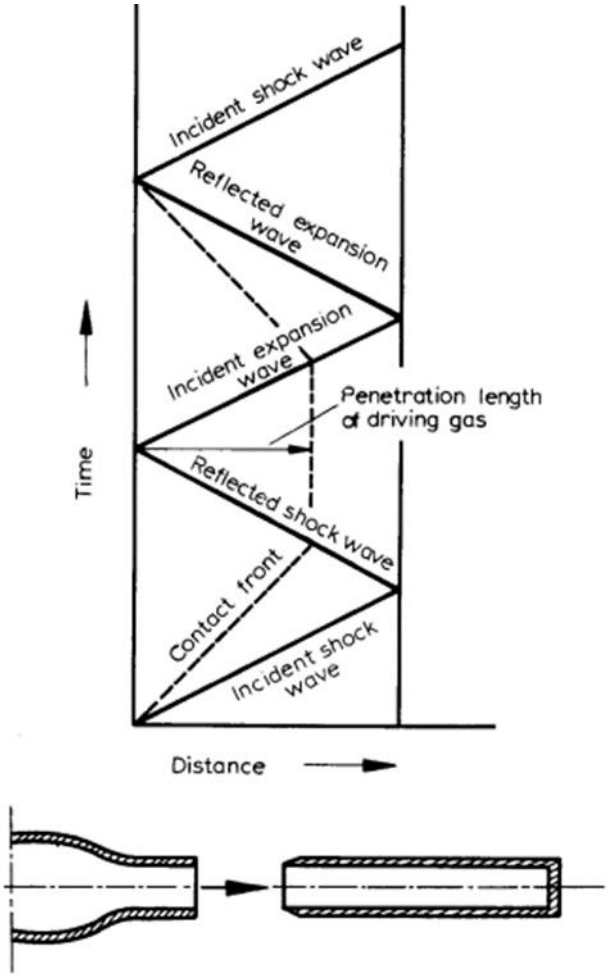

Figure 2.4: Wave diagram [8]

The next illustration (*Figure 2.5*) represents an enlargement of the first cell structure of the under-expanded jet flow. Edges, within which the cavity must be placed, are highlighted. For the reasons listed above, the nozzle-cavity distance must be between Xm relative to Mach disk position and Xc which represents the length of the first cell.[17]

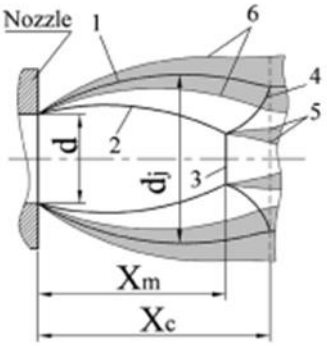

Figure 2.5: Under-expanded jet flow structure related to the first cell [17]

If the cavity entrance is very close to the Mach disc, it is possible to notice a further shock oscillating at high frequency. The latter is classified as the third operation mode of the resonator and it is defined as Jet screech.[14]

A compression cycle is schematised in the following F*igure 2.6*: in part A the compression waves entering the cavity are visible and, in following sections they join together forming a shock wave that moves up to the closed end. After they have reached it, these waves are reflected as shown in part F.[14]

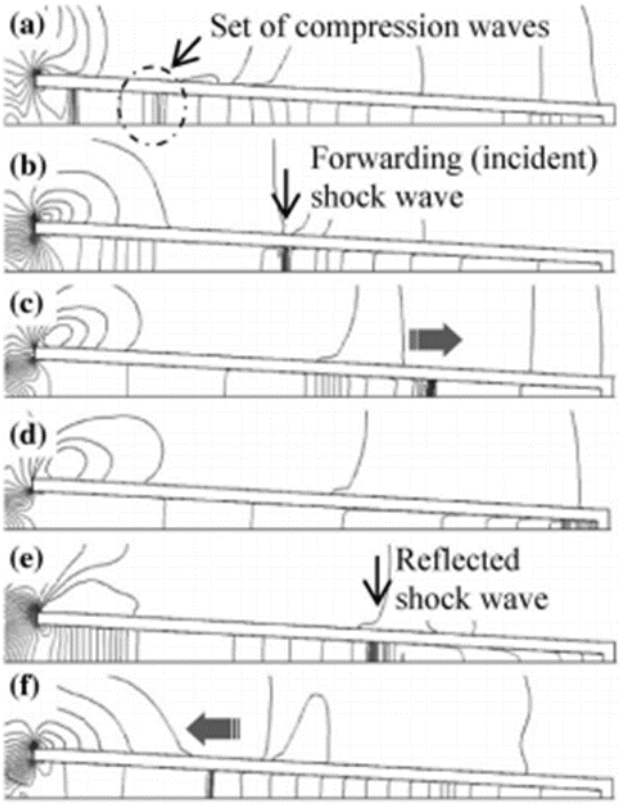

Figure 2.6: Compression cycle inside the resonator cavity [14]

A process of heating finally occurred because part of the gas has been trapped inside the resonator undergoing several compression cycles becoming increasingly hot. In this way, the temperature level reached in the cavity will be determined by the intensity and frequency of the shock waves present in the resonator.[1]

Due to the variation of the position of the cavity respect to the under-expanded jet flow outgoing from the nozzle, the temperature reached will inevitably vary and will not be constant, as shown in *Figure 2.7.*[1]

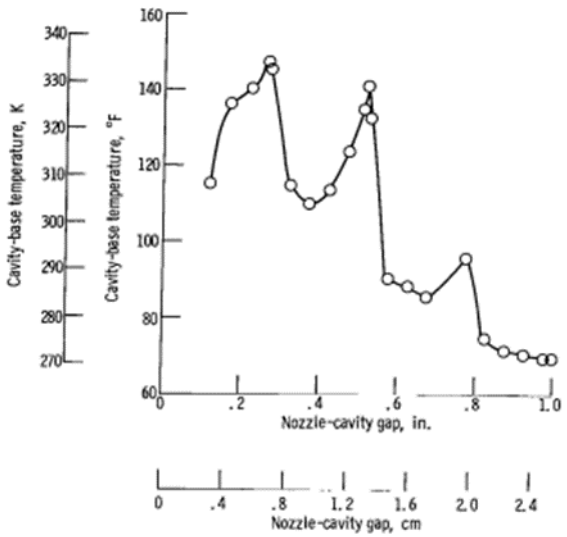

Figure 2.7: Base-cavity temperature as a function of the nozzle-resonator distance [1]

In *Figure 2.7* are highlighted the temperature peaks that correspond to instability areas described above. In particular the trend is decreasing with the corresponding increase of the distance, so it is important for thermal effects to identify the position of the first instability area.

2.2 Operating Modes

It was demonstrated by Sarohia and Back that for a resonator geometry there are three operating modes during which the thermal mechanisms are more or less accentuated.[5]

2.2.1 Jet Instability Mode

Jet Instability operating mode (JIM) occurs only with subsonic flow, for a wide range of nozzle-resonator distances and with a pressure ratio lower than 1.9.

In JIM, toroidal vortices are formed, which grow in size and speed proceeding downstream until the cavity inlet is reached. Inside the resonator the effects are minimal, in fact only weak compression waves are formed and thermal phenomena do not occur.[2]

Frequently, oscillations of such vortices have a frequency that can be superimposed on the fundamental resonance frequency and the interaction of

toroidal vortices with the cavity entrance produces pressure pulsations inside this one.[10]

2.2.2 Jet Regurgitant Mode

Jet Regurgitant Mode (JRM) occurs both with subsonic and supersonic flow, in this mode it is possible to define an operating cycle at the fundamental frequency of the resonance tube.[2] JRM cycle consists of two phases, the first is the inflow phase in which the gas enters the resonator and second is the outflow or exhaust phase.

In particular, the resonant frequency of the cavity can be obtained with the following formula:[2]

$$f = \frac{c}{4L}$$

In this formula, f represents the fundamental frequency, c is the average sound speed at the resonator inlet, L is the length of the cavity and number 4 is a parameter (it varies between 2 and 4 depending on resonator shape, in particular it is equal to 4 for cylindrical cavities with only one opening and 2 for completely conical cavities).[14]

The experimental results showed that for long resonators the oscillation frequency is near to the fundamental frequency of the cavity, while for the short ones the equation used is not very accurate.[14]

From the analysis of the under-expanded jet structure it emerged that the shock position is less than the distance between the nozzle outlet and the resonator inlet. During the first phase, the inflow phase, a large part of the gas enters the resonator, moreover the shape of the front shock will be different depending on the value of the pressure ratio. The incoming flow generates compression waves that proceed towards the closed end of the cavity. It is important to emphasise that if the length of the resonator is sufficient, the compression waves will join together forming a shock.[5,2] Once the waves have reached the cavity end wall, they are reflected towards the inlet [5,2] where an expansion front will finally be formed. These waves move inside the resonator, determining the transition from the inflow to the discharge phase.[2]

Expansion waves cause a negative pressure gradient behind the same front and, therefore part of the gas contained in the cavity of the resonator will exit forward. A collision occurs between the cold flow coming from the nozzle and the hot one from the resonator, generating an interface. Varying the intensity of one of the two flows, this separation line will move towards the nozzle or towards the resonator.[2]

As for the compression waves, the expansion waves are also reflected after reaching the bottom of the cavity up to the entrance of the same, thus concluding the discharge phase.

As mentioned before, the position of the interface depends on the intensity of the two flows, consequently after the discharge phase has ended, a weakening phenomenon of the flow coming from the resonator can be detected, which causes the displacement of this boundary towards the cavity, ending the cycle.[2]

For a pressure ratio between 1.9 and 3.4, a shock diamond structure is formed downstream of the nozzle, while for values greater than 3.4 a Mach disk appears which increases its strength with increasing pressure ratio.[2]

JRM Thermal Phenomena

In Jet Regurgitant Mode, as previously described, the resonator compresses the gas trapped in the final part of the cavity; after that an outflow phase occurs in which the gas escapes from the resonator and then the trapped one decompresses. The heat is generated by the isentropic shocks that are present inside the resonator and by the friction along the walls. However, the performance is limited in terms of maximum temperature that can be reached in this mode because a mass exchange occurs between the incoming cold flow from the nozzle and the hot flow out of the resonator. Another factor is the convection along the cavity walls since they are periodically heated and cooled due to the presence of the two hot and cold flows.[4]

The heat balance is as follows:[4]

$$Q_{Massexchange} + Q_{Convection} = Q_{Isentropicshockwave} + Q_{Friction}$$

2.2.3 Jet Screech Mode

Jet Screech Mode (JSM) occurs only with supersonic flow. Every time the nozzle-resonator spacing becomes equal to that of the free-jet shock position, there is the transition between Jet regurgitant mode and Jet screech mode. A normal shock is created between the outlet of the nozzle and the inlet of the resonance tube oscillating at high frequencies. It should be remembered that the flow at the nozzle outlet is not affected by the presence of the resonator.[2]

The shock strength and its frequency depend on the nozzle-resonator distance, the nozzle pressure ratio and the shape of the cavity inlet.[2]

In this mode it is possible to reach higher temperatures because the cold flow cannot enter the resonator cavity.[2]

To better highlight the difference between JRM and JSM, see the following *Figure 2.8,* where the shock position (Xs/d) is indicated as a function of the pressure ratio. This shock is positioned between the nozzle outlet and the resonator inlet.

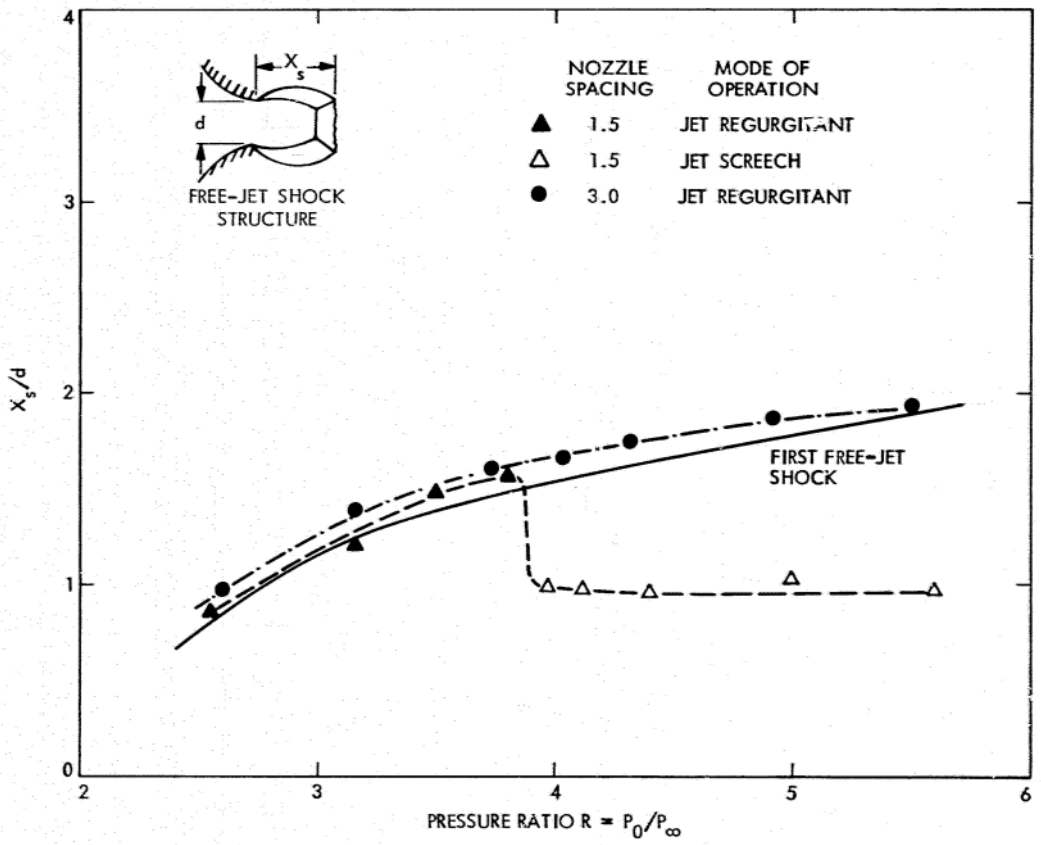

Figure 2.8: Difference between JRM and JSM [2]

The solid line indicates the free jet shock position. The experimental points, obtained with a spacing s / d = 1.5 up to a pressure ratio of 3.9, indicate the shock position Xs/d during the inflow phase of the JRM. These points are comparable to the free jet shock position, that is why it can be said that the resonator in this phase is irrelevant. Once the pressure ratio of 3.9 is exceeded the system switches to JSM mode, at that point the jet shock position is equal to the spacing s / d. A normal shock is formed in front of the resonator input which oscillates at high frequency. By further increasing the pressure ratio, the constant spacing is less than the free jet shock position and therefore it remains in the JSM mode.[2]

With an increase in spacing (s / d = 3) the experimental points are superimposed on the free flow shock position and there is no transition to the JSM since the nozzle-resonator distance is greater.[2]

JSM Thermal Phenomena

As previously mentioned, high temperatures are reached in Jet Screech mode, because cold flow cannot enter the cavities due to the shock that is formed in front of its entrance. The latter traps the gases present in the resonator subjecting them to continuous compressions with the consequent increase in temperature.[4] Therefore, as a result of this mechanism which determines a smaller mass flow in the resonator, there is a lower mass exchange and a lesser heat developed by friction. As soon as the shock vibration becomes equal to the fundamental frequency of the resonator, high temperatures are reached.[4]

The heat balance is as follows:[4]

$$Q_{Massexchange} = Q_{Isentropicshockwave} + Q_{Friction}$$

2.3 Parameters Affecting Resonator Performance

There are many studies aimed at understanding which are the most important parameters in the design of the system and which one are indispensable to carry out the tests correctly. Phillips and Pavli in 1971 have performed a study in which various factors and their effects have been listed as follow:[1]

- Nozzle pressure and NPR (Nozzle Pressure Ratio)
- Nozzle-cavity distance
- Cavity shape
- Resonator cavity length
- Gas composition
- Cavity material
- Cavity thermal insulation effect
- Resonator and nozzle diameter
- Wire application effect in front of resonator inlet

In the following paragraphs these parameters will be described in detail.

2.3.1 Nozzle Pressure and NPR (Nozzle Pressure Ratio)

The NPR parameter is of considerable importance in the tests carried out:

$$NPR = \frac{p_n}{p_e}$$

In the formula, p_n represents the nozzle total inlet pressure and since the isentropic expansion is considered, this parameter corresponds to the total pressure of the free jet, p_e is the static pressure downstream of the nozzle.[5]

From the experimental evidence it emerged that the pressure waves at the cavity base have higher amplitudes with increasing nozzle pressure.[1] The results are shown in the graph in *Figure 2.9*, where for different NPR values the amplitude of the pressure waves at the cavity base is related to the nozzle pressure.

From the figure, the optimal NPR value is around 4.5 since the wave amplitudes are greater than those corresponding to NPR 6 and 8. Furthermore, this difference becomes more marked with higher nozzle pressures. Finally, for each NPR value, a linear variation of the amplitude with the nozzle pressure was detected.

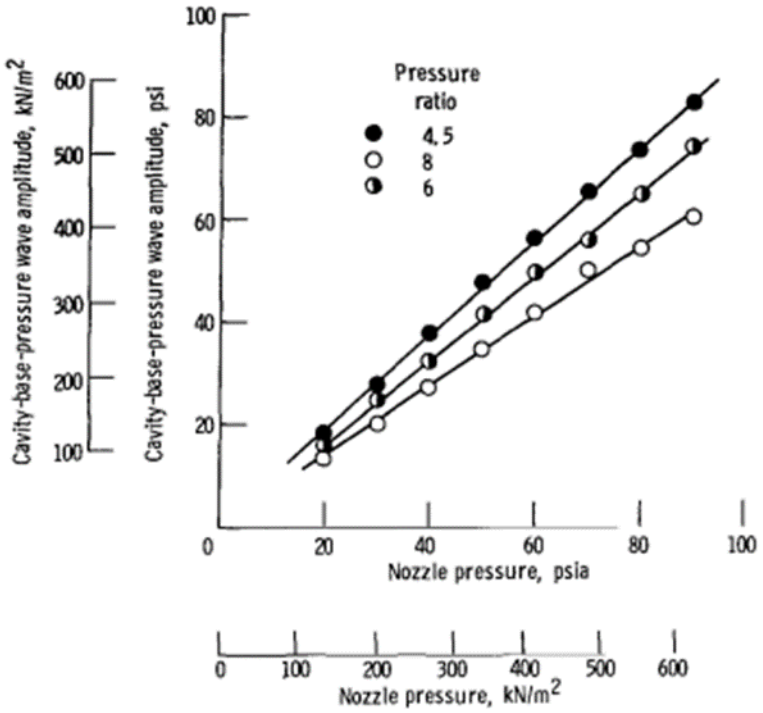

Figure 2.9: Cavity-base-pressure waves amplitude in relation to the nozzle pressure for different NPR values, test performed with nitrogen [1]

Similar conclusions can also be deduced from the following graph in *Figure 2.10* in which the temperature at the cavity base is compared with the NPR pressure ratio, using different nozzle pressure values as an additional parameter.

It is possible to notice that as the nozzle pressure increases (starting from 2.07 bars up to 6.20 bar) temperatures recorded at the cavity base increase too, this means that for higher nozzle pressures, the amplitude of the compression waves at the end-wall increases. To conclude, when the pressure of the nozzle changes, the point on the abscissa where the maximum temperature is observed does not change, at approximately NPR = 4.5, confirming what has been said previously.[1]

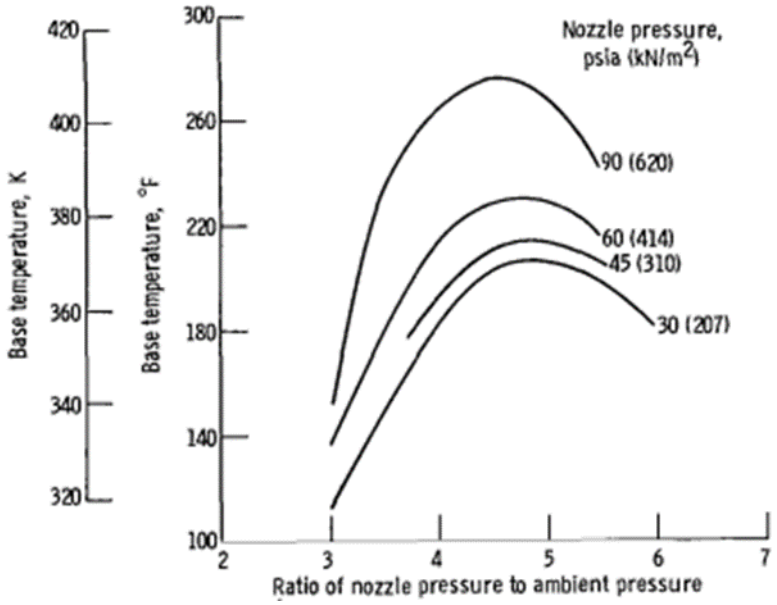

Figure 2.10: Cavity base temperature as a function of NPR for different nozzle pressure values [1]

2.3.2 Nozzle-cavity Distance

After considering all the processes that have been already explained before, it is important to remember that the resonance effect happens when the curved shock, previously formed in front of the entrance to the resonator cavity, has been placed inside one of the instability regions typical of an under-expanded jet flow.

As it has emerged, the cavity does not affect the shock structure and, with Nozzle-Pressure Ratio (NPR) increasing, instability regions moves away from the nozzle, as it is shown in the following graph of *Figure 2.11,* which represents the position of the first cell relative to the instability zone for different NPR values.[1] It is noted that for higher pressures corresponding to higher NPRs, the position of this cell moves away from the nozzle and approaches the resonator cavity.[1]

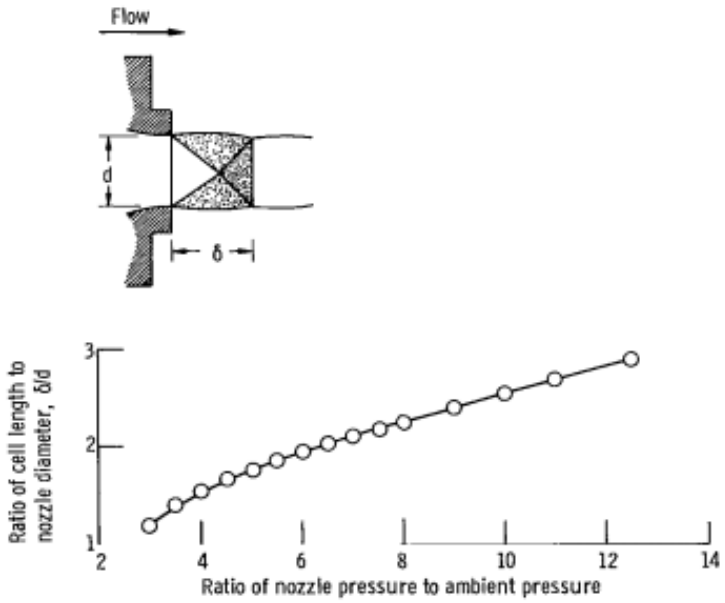

Figure 2.11: Variation of position of the first under-expanded flow cell in relation to NPR [1]

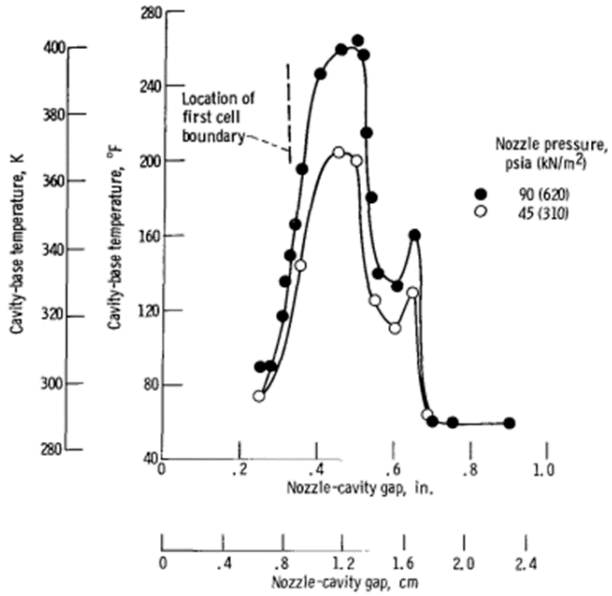

Figure 2.12: cavity base temperature in relation to nozzle-resonator distance [1]

The data shown in *Figure 2.12* is related to the temperature at the cavity end-wall. These results are a function of distance between the nozzle and the resonator and they have been obtained in relation to two different nozzle pressure values.[1] At the same NPR ratio, the temperatures reached are higher with higher nozzle pressures as confirmed later by observing the influence of other parameters. For both pressure values, maximum temperature is found at a gap of 1.14 cm. Due to

the relevance, as mentioned, to place the shock inside the jet instability cell, its position is shown by a dotted line on the graph. As it can see, the temperature peak is detected at a slightly higher distance, this is because the curved shock formed in front of the resonator cavity, is located at a certain distance from it, hence the subtle discrepancy.

From this test, carried out using nitrogen as a gas,[1] it emerged that the parameters influencing the position of the temperature peak are the nozzle diameter and the nozzle / ambient pressure ratio, i.e. NPR.

However, if both parameters remain unchanged, the optimal position does not shift as the nozzle pressure changes, as evidenced by the two values of 6.2 bar and 3.1 bar shown in the graph.[1] The second peak detected in temperature could refer to the position of the resonator within the second zone of instability which provides a smaller increase.

2.3.3 Resonator Cavity Shapes

Until the discovery of the phenomenon in 1919 to the recent tests, numerous configurations have been tested.

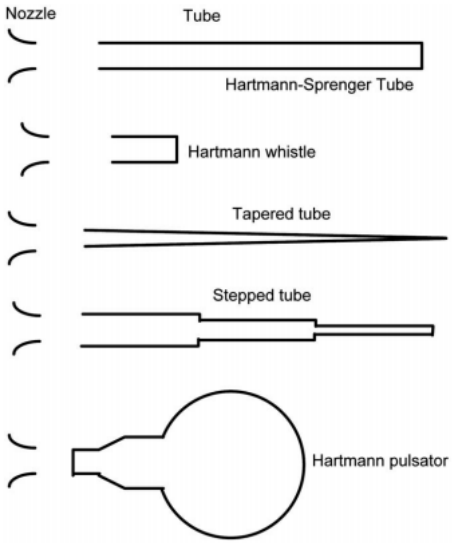

Figure 2.13: Resonator shapes, from the first attempts to the latest variants [10]

In *Figure 2.13* is evidenced the shapes used in Hartmann's first experiments, whose interest was linked to the sound generated and not to the thermal effects that have been discovered later.

The cavity shapes applied to the study of thermal effects are the classic cylindrical, stepped and conical. Referring to the "thermal" resonator and not to the one for

sound effects, the experimental setup has been named Hartmann-Sprenger tube.[3]

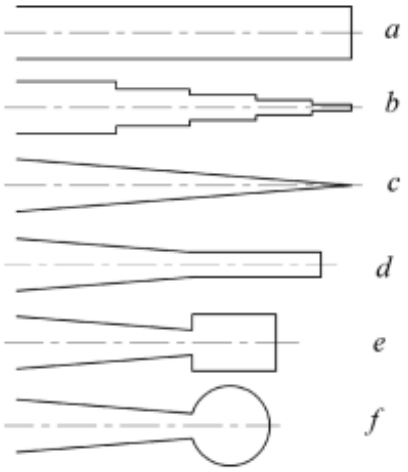

Figure 2.14: Later shapes used for the resonator cavity, with particular geometries such as conical and cylindrical or conical and spherical [17]

The diagram in *Figure 2.14* depicts some new shapes of the resonator cavity, in addition to the first three "classic" ones (i.e. cylindrical, stepped and conical), more complex cavities are added, this means that attempts to find more performing geometries are still proceeding.

From the tests carried out comparing two different cavities, it emerged that the temperature reached with the cylindrical one is lower than that of the conical cavity as shown in *Figure 2.15* where a significant discrepancy is highlighted.[1]

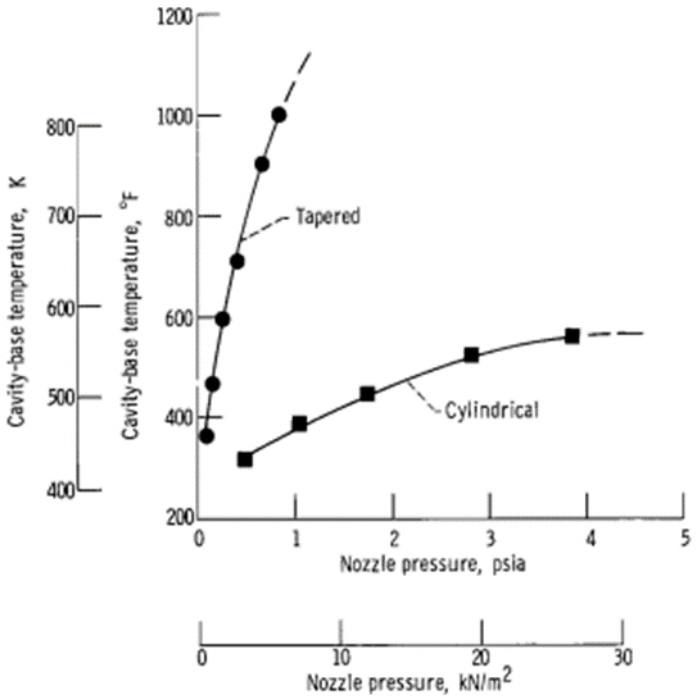

Figure 2.15: Cavity base temperature comparison for two different resonator shapes [1]

In this experiment, hydrogen has been used as a gas, and the clear superiority in terms of heating of the resonator conical shape have emerged,[1] however it is constructively difficult to produce it. This problem has been partially solved through additive manufacturing or by using a stepped cavity, which allows for intermediate performance similar to the conical shape and it is easier to build.

Table 1 Temperature measured after 100 ms

Gas	Cavity temperature (°C)		
	Cylindrical ($L/D = 20$)	Stepped (1)	Stepped (2)
Nitrogen	167	372	218
Argon	290	512	327
Helium	480	928	564

Driving pressure = 7 bar

Figure 2.16: Maximum temperature results for cylindrical and stepped cavities with different gases [8]

This table in *Figure 2.16* shows the results of the Brocher and Ardissone experiments in 1983. Comparing the stepped and cylindrical cavities, the best performances are obtained with the former because higher temperatures can be obtained.[8]

Using the conical shape it is possible to add a cylindrical extension at the front as in *Figure 2.17*. The results, however, showed less performance, in fact, with the increase in the length of the cavity, the frequency of the oscillations decreases and, therefore, the recorded temperature too.[1]

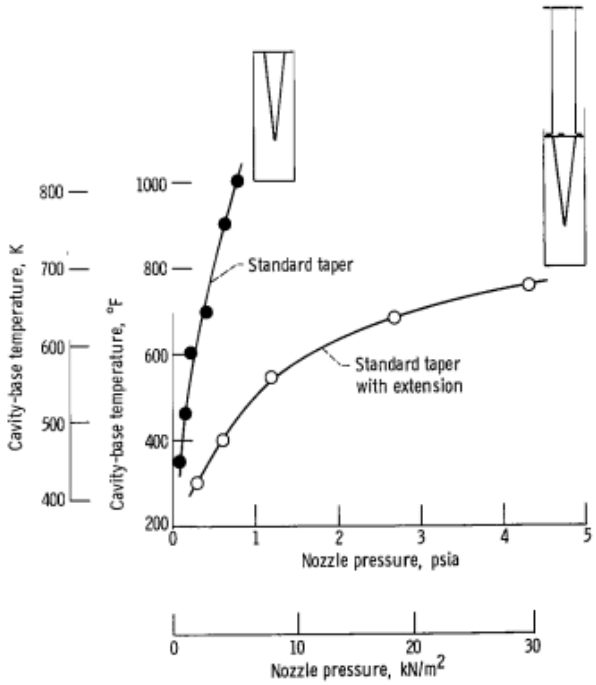

Figure 2.17: Conical resonator cavity with added cylindrical extension [1]

Finally, it is possible to state that the conical and stepped resonator cavities have been found to be the most efficient ones, as demonstrated by some studies including Kupsv and Filitov in 1981, Marchese in 1974 and Phillips and Pavli in 1971. It has also been experimentally demonstrated that the optimal value of the taper angle is 6 degrees.[17]

2.3.4 Resonator Cavity Length

From the resonator study has emerged that the cavity depth affects its mode of operation. In fact, its variation determines changes in the path of the compression waves or shocks, which can join or not depending on the resonator length.[1]

It has also reported that the length of the cavity changes the frequency of the resonance oscillations, studies by Hartmann and Trolle suggested a length of 1-2 times the diameter of the resonator as an optimal value [10] while Kastner and Samimy have observed that amplitude corresponding at the fundamental frequency decreases with length increase,[10] to finally reach the temperature at the bottom of the cavity, which tends to increase with increasing nozzle pressure at the same pressure ratio (NPR).

The experimental results showed that a short cavity performs better because with a greater length of this latter, the resonator surface subjected to heat exchange increases, as well as the losses due to convection and conduction lowering the wall temperature.[1] Therefore, according to the 1971 conclusions, the tests should be carried out considering an optimal cavity length between 4.76 cm and 9.68 cm.[1]

These conclusions are determined from the results of *Figure 2.18*, which shows the effects of the cavity length with a cylindrical resonator. For the two values considered optimal (4.76 cm and 9.68 cm) the higher temperatures are reached and the trends are superimposable, while for longer cavity lengths the performances are lower.

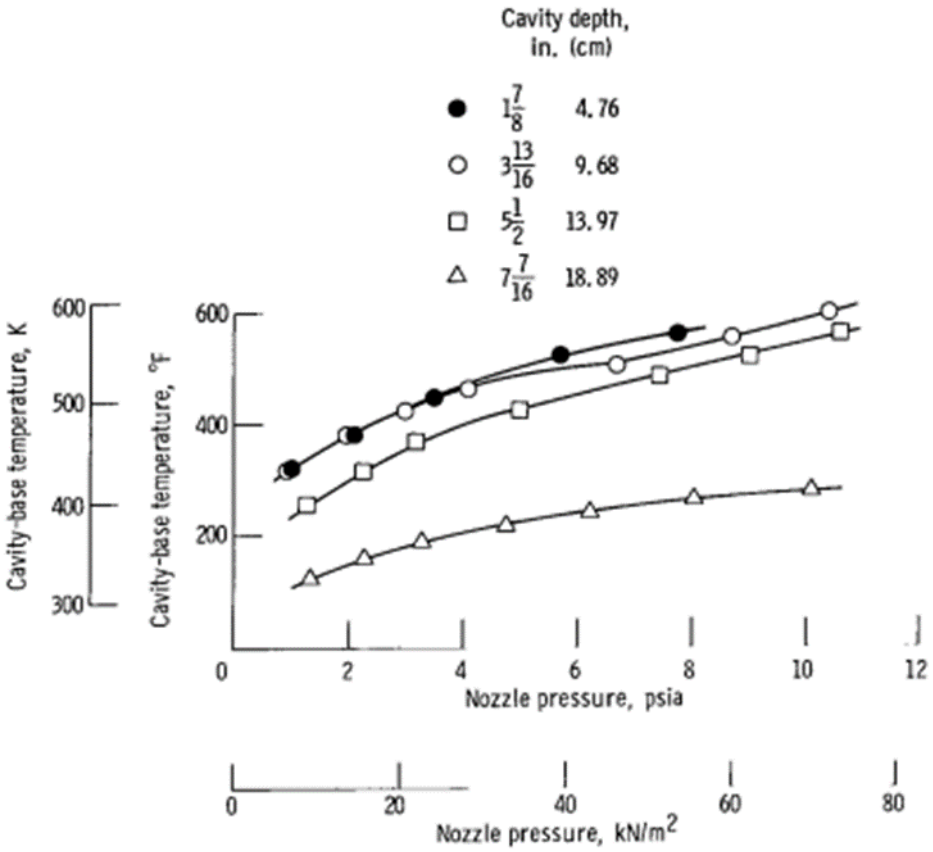

Figure 2.18: Cavity base temperature for different cavity depths [1]

2.3.5 Gas Composition Effect

Among the different gases used for the tests, hydrogen provides better performance than nitrogen by reaching higher temperatures at the bottom of the cavity, followed by oxygen with a similar behaviour.[1]

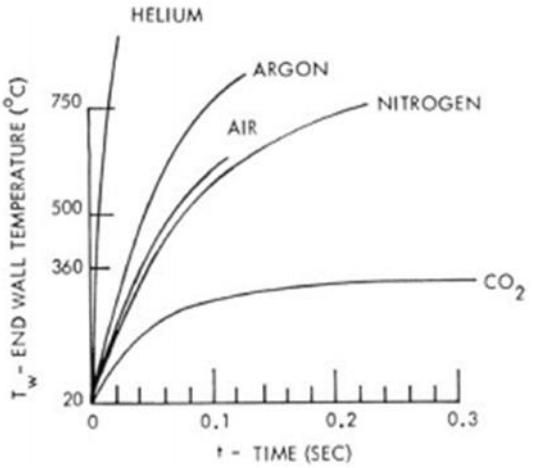

Figure 2.19: Effect of gases on the end-wall temperature [5]

From a performance point of view, air, often applied in tests including those that have been developed in our laboratory, has characteristics between nitrogen and argon as shown in *Figure 2.19*. Carbon dioxide provides poor performance while significant heating effects are recorded for helium.

Since hydrogen seems to provide higher temperature values, after the analysis of the frequency of the oscillations inside a resonator fed with this gas, it turned out that these oscillations are 3-4 times higher than those of nitrogen, which means a greater release of energy per unit of time and therefore an increase in temperature at the cavity base.[1]

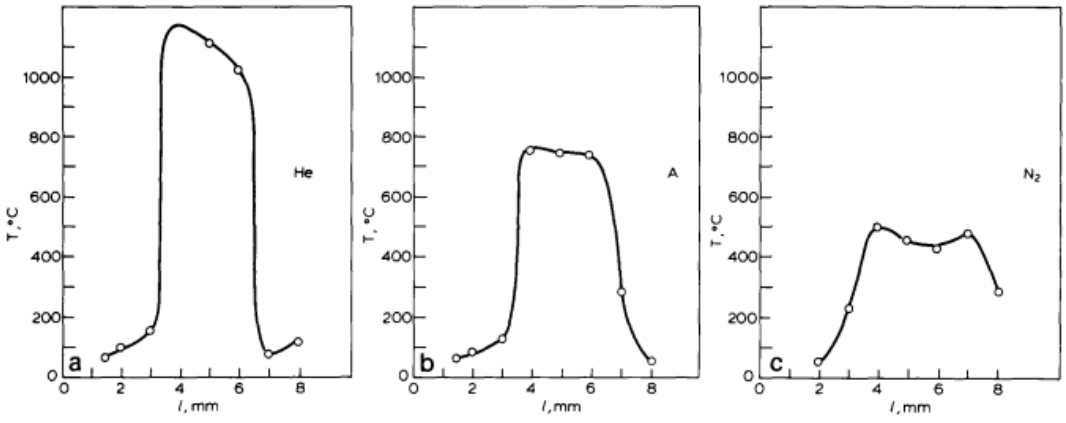

Figure 2.20: Maximum temperatures reached by different gases as a function of nozzle-resonator distance [8]

Similar conclusions are shown in the graphs of *Figure 2.20* where helium allows to reach higher temperatures followed by argon and nitrogen, confirming the trend

of the previous figure [8]. Especially, argon reveals a visible interval in which the temperature remains almost constant with only slight variations as the nozzle-resonator distance varies, this trend has been also confirmed in our tests performed with constant distance and variable NPR.

2.3.6 Cavity Material

The resonator must be built with material characterized by low thermal conductivity, in this way the heat losses between the gas and the resonator walls are minimized. It must also be waterproof and structurally robust.[1]

From Brocher and Maresca study of 1972 it appears that roughness affects the maximum temperatures obtainable especially for small cavities where higher values were recorded for resonators with greater roughness than those with smooth walls.[21]

Materials used in the various experiments:[1,8]

- Wood: used for a single ignition, very low thermal conductivity
- Zirconia: problem for porous structure
- Asbestos: composite whose characteristics vary according to the percentage of binder used
- Durestos: composite with asbestos fibres and phenolic resin
- Machinable ceramic: higher thermal conductivity, it can be used for applications that require several ignitions, however it is fragile

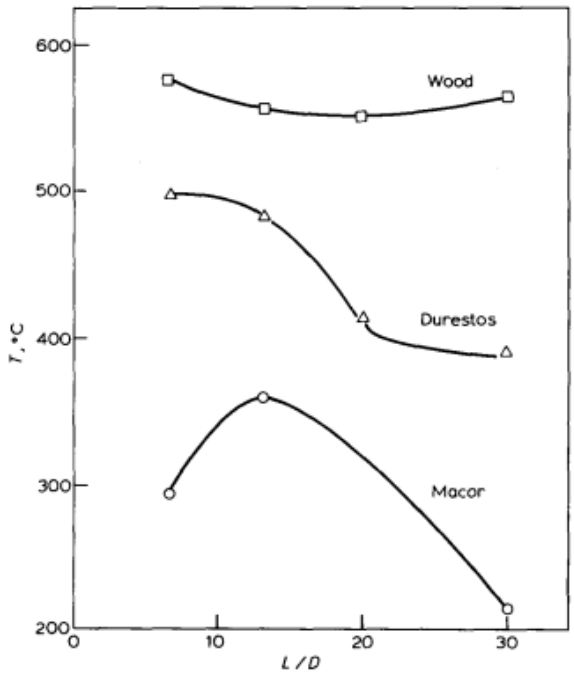

Figure 2.21: Temperatures reached for different materials [8]

The temperatures reached will therefore be different not only for the various cavity shape but also for the different material. *Figure 2.21* shows the temperature trends for some examples: materials with low thermal conductivity, such as wood, allowed to obtain high temperatures.[8]

As a result of the longitudinal temperature gradient, there is a heat flow along the resonator wall. To reduce these heat losses, the walls must be thin or made of a material with low thermal conductivity. In fact, from *Figure 2.22* it is evident that the application of a cavity with a smaller wall thickness allows to reach higher temperatures at the bottom of the cavity.[17,21]

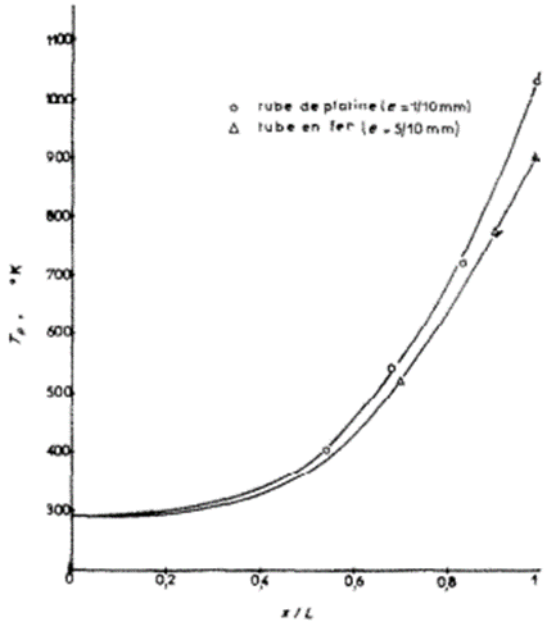

Figure 2.22: Comparison of temperature trends for two cavities with different thickness [21]

Finally, to reduce convection heat losses, the part of the resonator subjected to heating can be covered with an insulating container or special screens as it has been done in the studies of Kessaev and colleagues in 2001, Kupsov and colleagues in 1977 and Phillips and Pavli in 1971.[17]

2.3.7 Cavity Thermal Insulation Effect

In order to evaluate the reduction of convection and radiation of the resonator external wall, it has been thermally insulated with glass wool during an experiment in 1972. The results showed that for large cavities the effects are very marked, while they are lower for small resonators such as those used in our tests.[21]

Figure 2.23 shows temperatures trend inside the resonator with and without thermal coating subjected to a supersonic flow regime, a temperature increasing of 120 ° C on the end wall has been recorded compared to the cavity without coating.[21]

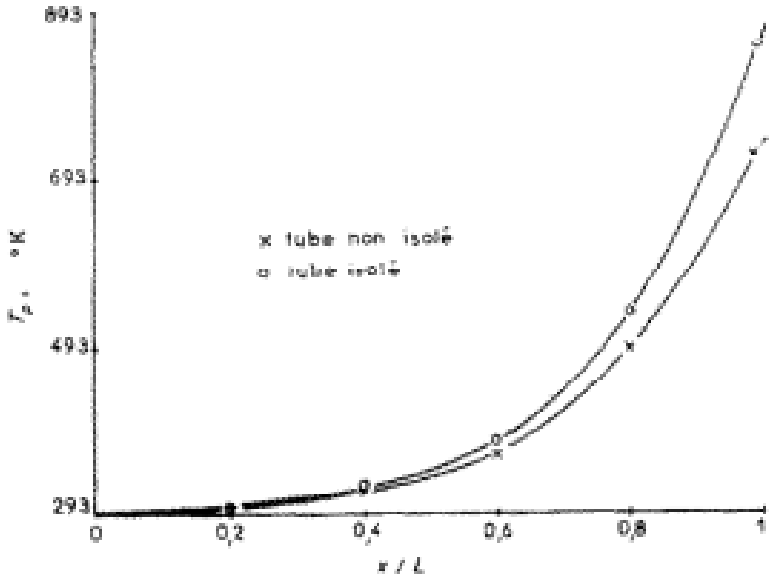

Figure 2.23: Effect of thermal insulation on the iron resonator

(l/D = 2.4, To=298°K, M = 2)[21]

2.3.8 Resonator and Nozzle Diameter

Hartmann initially has suggested that the dimensions of the resonance tube must be similar to those of the nozzle, while Palme has stated that the diameter of the cavity itself must be equal to the largest diameter reached by the under-expanded jet structure. Studies by Monson and Binder suggested a ratio of 1.27 between cavity and jet diameters.[10]

To better clarify those aspects, a further benchmark that could be considered is the ratio between the nozzle and resonator cavity diameters: the studies showed that an optimal range is between 1.1 and 2.5.[4] In particular, in the first Hartmann's studies of 1922 the nozzle diameter was equal to that of the resonator. Subsequently for thermal systems some studies have considered more performing values in which the diameter of the nozzle was smaller than that of the resonator cavity.[1] Other tests are the ones of Phillips and Pavli in 1971, in which a value of 1.25 was established. Strabinsky in 1973 chose 1.3 as a parameter,[17] the same value of the one chosen by Shapiro,[4] 1.33 by Marchese in 1974, a range between 1.3 and 2.5 by Butorin and colleagues in 1988 and 1.1-1.6 gap by Kessaev and colleagues in 2001.[17]

As it can be observed, there is no unique optimal value. In each experimental setup, it is possible to obtain the one that best suits the configuration in order to reach a higher temperature at the cavity bottom.

2.3.9 Effect of a Wire placed in front of the Cavity Inlet

In order to raise the maximum temperature peak at the cavity bottom, some tests were carried out by applying a metal wire in front of the resonator; however the outcome was negative, penalizing the performance.[1] For example, the study by Phillips and Pavli in 1971, during which a steel wire with a diameter of 0.079 cm has been placed transversely in front of the cavity opening.[1] The results obtained, as mentioned at the beginning of the paragraph, were negative, in fact as shown in the following graph (*Figure 2.24*) pressure amplitude at the bottom of the cavity is smaller than the same without disturbing element for different distances of steel wire from cavity inlet, consequently also the recorded temperatures are lower.[1]

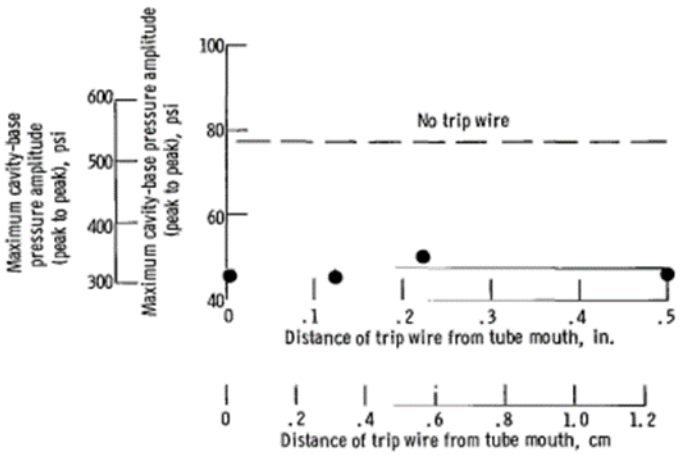

Figure 2.24: Pressure amplitude recorded at the cavity bottom in relation to the distance of wire from inlet of this one [1]

However, the conclusions of other studies have not been the same, in fact Sprenger in 1954 detected an increase in temperature with the application of a nylon cord with a diameter of 0.001 cm placed after the exit of the nozzle; a cylindrical resonator was used with a diameter of 0.3 cm and a length of approximately 10 cm.[19]

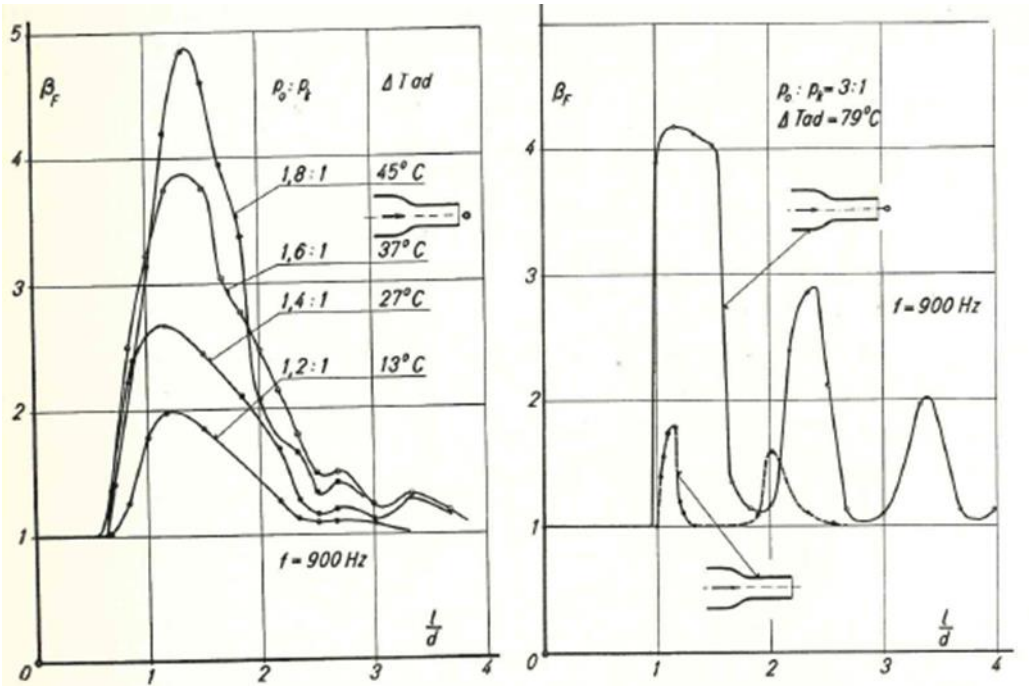

Figure 2.25: Pressure and temperature variation effects with disturbance element application, Sprenger's experiments of 1954 [19]

The examples of *Figure 2.25* show the results of the tests carried out by Sprenger with the use of an obstacle placed in front of the nozzle.

The graph on the left indicates the effect of the pressure variation. For the four values reported, the nozzle outflow speeds are between Mach numbers 0.5 and 0.95. As the pressure ratio increases, the temperatures also increase while the l / d parameter has not been much affected, in fact the maximum peak occurs in approximately the same position as the pressures vary.[19] Finally, the graph on the right shows a comparison of the temperatures reached with and without the use of nylon filament at the same pressure ratio, the difference is clearly visible.[19]

Positive results in the application of objects placed between the nozzle and the cavity have also been found in the 1962 study by Vrebalovich. Through the use of a resonator with a cylindrical steel cavity placed in a wind tunnel with supersonic flow, elements called tripping devices were added near the cavity inlet, in particular an obstacle with an annular shape and one with airfoil shape.[20]

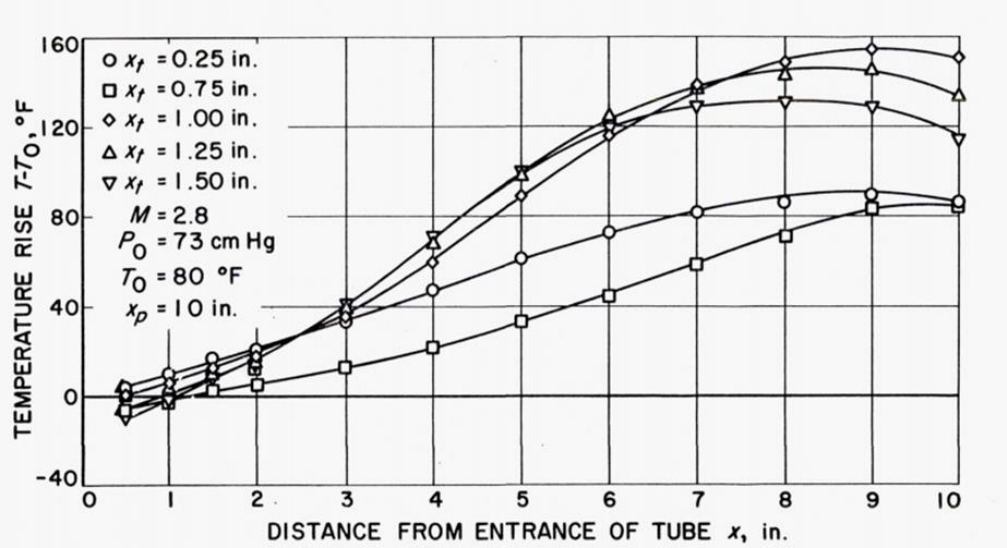

Figure 2.26: Temperature variation inside the cavity as a function of the positioning of the annular tripping device [20]

One of the main parameters in this type of test is the distance of the disturbing element from the cavity entrance. In *Figure 2.26* this distance is indicated with X_t, while X_p is the thermocouple location at the cavity bottom. This test was carried out with the annular tripping device and the optimal value is the one with positioning of the disturbing element at X_t = 1 in. = 2.54 cm from the resonator inlet.[20]

In order to evaluate the effectiveness of the two forms used on the temperature variation, the following graph is shown (*Figure 2.27*). Keeping the distance of the tripping device constant and equal to 0.75 in., a significant discrepancy emerges between annular and airfoil shapes with better results for the latter.[20]

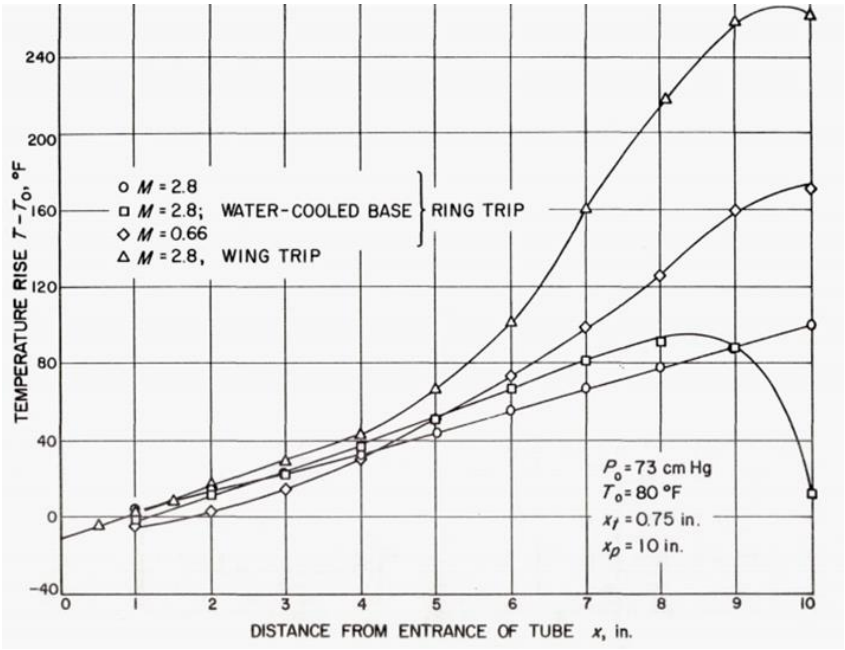

Figure 2.27: Temperature trends for different tripping devices [20]

Chapter 3

Experimental Results

After having explained the resonance phenomenon in the previous theoretical sections, from its origins to its functioning and having listed the most influential parameters, let's now move on to the experimental section.

The used setup will be described initially, and then the results will be displayed in terms of the maximum temperature reached at the cavity bottom and the frequency peaks through the FFT graphs.

As observed in the theoretical discussion, the most suitable resonator shape is the conical one, therefore in our tests this shape was used in a very thorough way and the results obtained will be used to refine the setup for subsequent tests.

At the end of these studies a different cavity will be designed for comparison, while other elements will be applied to the same cavity used during the first test campaign with the same objective.

3.1 Description of the Experimental Apparatus

Figure 3.1: Experimental setup

The first setup used is the one shown in *Figure 3.1* where the wooden platform can be seen. It is used as a fixing base for the nozzle and the resonator. The nozzle is free to move and be locked allowing the adjustment of the s / d parameter.

It is also fundamental to check that the nozzle and the resonator are perfectly coaxial. An error in the alignment may cause a considerable decrease in the maximum attained temperature, therefore this wooden structure is a unique

piece and it is not possible to separate the resonator section from the nozzle one to vary the s / d parameter; to obtain this variation the nozzle is moved by translation, in this way coaxiality is granted.

With reference to *Figure 3.1*, the compressed air supply line is visible on the left. A pressure gauge with a filter is present to collect air moisture coming from the compressor.

This manometer provides the pressure values used as a reference for the various NPRs in order to evaluate the maximum achievable temperature peak and draw conclusions on the "optimal" parameters, comparing them with the results of other studies.

The air comes from a tank at a pressure of 9 bar, however, as a result of the various losses along the line, this value cannot be obtained at the nozzle inlet. In fact, according to the tests carried out, the maximum relative pressure considered was 5.5 bar, corresponding to an NPR of 6.5. In order to evaluate the phenomenon with upper pressures, the manometer in front of the nozzle was removed; this allowed to reach higher values up to 8.6 bar.

A problem encountered during the early stages of the experiment concerns the fixing of the thermocouple at the bottom of the resonator. In the initial phase it was decided to fix it using a washer as shown in *Figure 3.2*; after that the thermocouple was fixed more firmly using a copper wire, checking that the end of sensor was resting on the resonator to avoid errors in reading data.

Figure 3.2: Preliminary setup with the thermocouple blocked by a washer

In general thermocouples produce a temperature-voltage relationship as a result of the thermoelectric effect; then this voltage can be reinterpreted obtaining a temperature measurement.[22] Since they are used for different applications, the temperature ranges, which thermocouples are subjected to, can be very different and therefore there are many variations. Mainly the choice of the thermocouple is made on the basis of two important criteria: the temperature range and the sensitivity. Other criteria are: the use of chemically inert, magnetic or not magnetic materials.[22] A representation of the existing variants with the temperature limits can be seen in *Figure 3.3*.

In the tests a type K thermocouple was used; this variant is the most common, it is composed of two chromel-alumel alloys.[23] The first one is made up of nickel and chromium, while the second one of nickel, manganese, aluminum and silicone. The K thermocouple provides the widest temperature range (-200 ° C to 1260 ° C), good corrosion resistance, inexpensiveness and it works well in oxidizing environments.[22,23] However nickel, one of the constituent materials, is magnetic.[22,23] Other technical details are shown in *Table 3.1* below.

Temperature range	-200 °C a 1260 °C
Sensitivity	41 µV/°C
Wire temperature range	0°C a 200 °C
Melting point	1400 °C
Standard precision	+- 2.2 C%

Table 3.1: Technical data of a generic type K thermocouple [23]

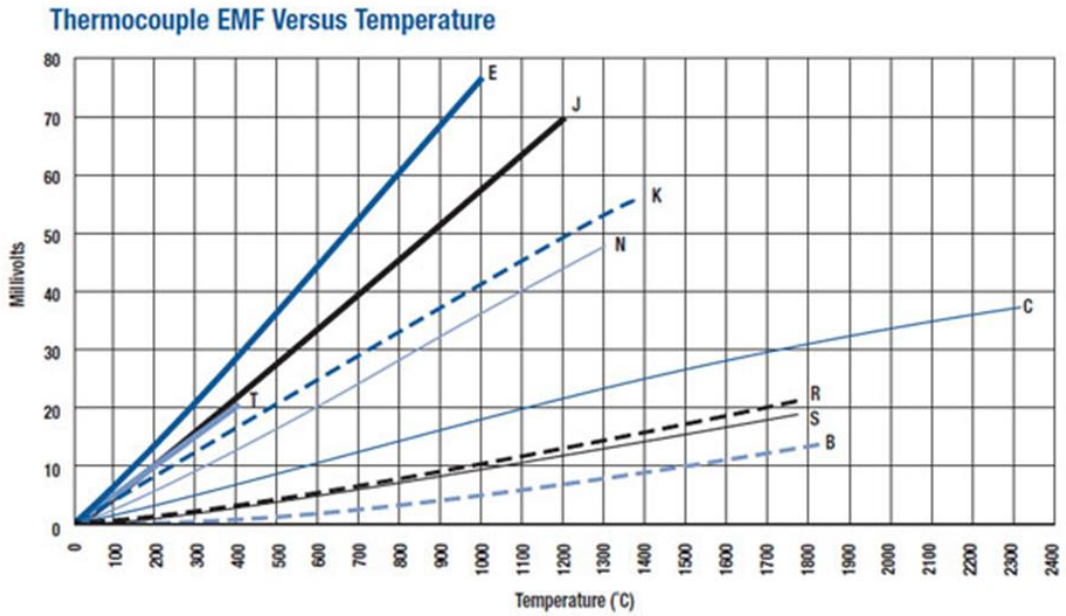

Figure 3.3: Graph of thermocouple types in relation to millivolts and measurable temperature range [23]

The resonator used is made of Inconel® created by additive manufacturing and it has a conical shape. In fact, as reported in various articles, this is the best shape from the performance point of view, even if it is complicated to build and as visible from the *photo 3.4* it has a rough finish surface.

Figure 3.4: Front view of 4 mm diameter circular nozzle outlet.

A 3D view of the used resonator and a table with the relative dimensions are shown in the following *Figures 3.5* and *3.6*.

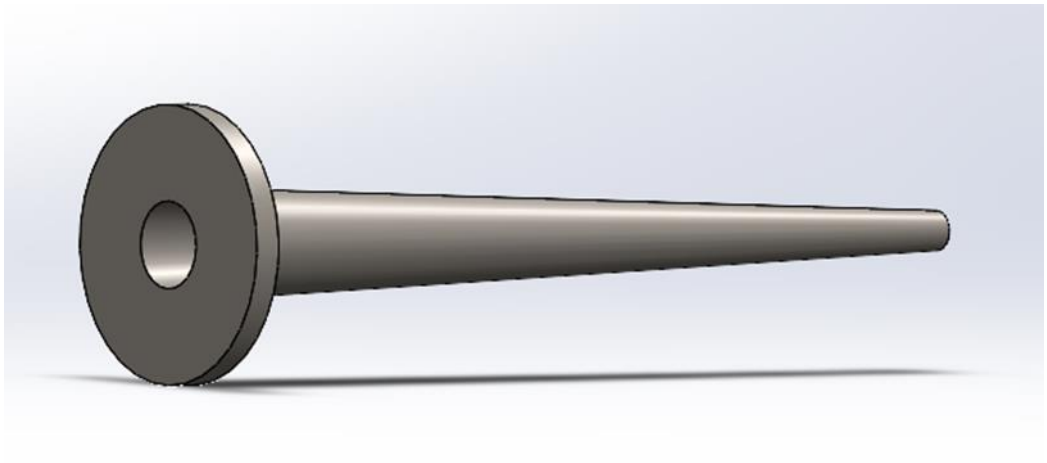

Figure 3.5: Conical resonator

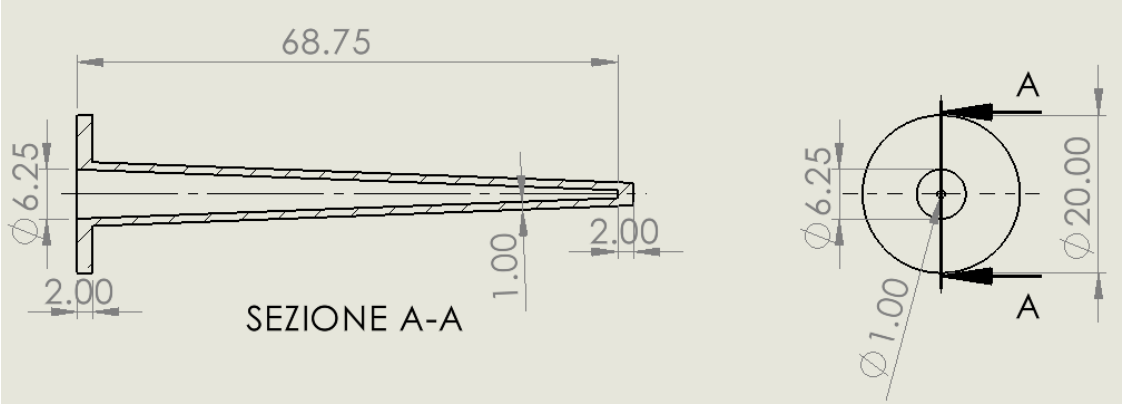

Figure 3.6: Conical resonator dimensions with section view

To complete the setup, a Logitech® Dialog 320 microphone was added in the immediate vicinity of the wooden support between the nozzle and the resonator inlet, to record the variation of the pressure waves and obtain the frequency spectrum through the analysis of the signal. With a range of detectable frequencies up to 16 KHz, the values obtained in our tests fall within this interval. The following *Table 3.2* shows some technical data.[24]

Frequency range	100 Hz up to 16000 Hz
Sensitivity	- 67 dB
Input impedance	2000 Ω
Microphone operating mode	mono
Audio input	uni-directional

Table 3.2: Logitech® Microphone Technical Data [24,18]

3.2 First Tests to Verify Operation

This paragraph shows the first tests carried out called respectively Test 1 and Test 2. The aim of these tests was to interface with the resonance phenomenon and verify the correct functioning of the experimental setup, finally to compare the results with those of other studies.

Test 1

Nozzle diameter (d)	4 mm
Nozzle-resonator distance (s)	10 mm
Relative pressure	4 – 5,5 bar
s/d	2.5

Table 3.3: First test data

With this value of nozzle-resonator distance, the maximum temperatures reached were recorded for the various relative pressure values.

Relative pressure [bar]	Temperature [K]
4	**680**
4,5	**850**
5	**870**
5,5	**886**

Table 3.4: Temperatures recorded for the first test

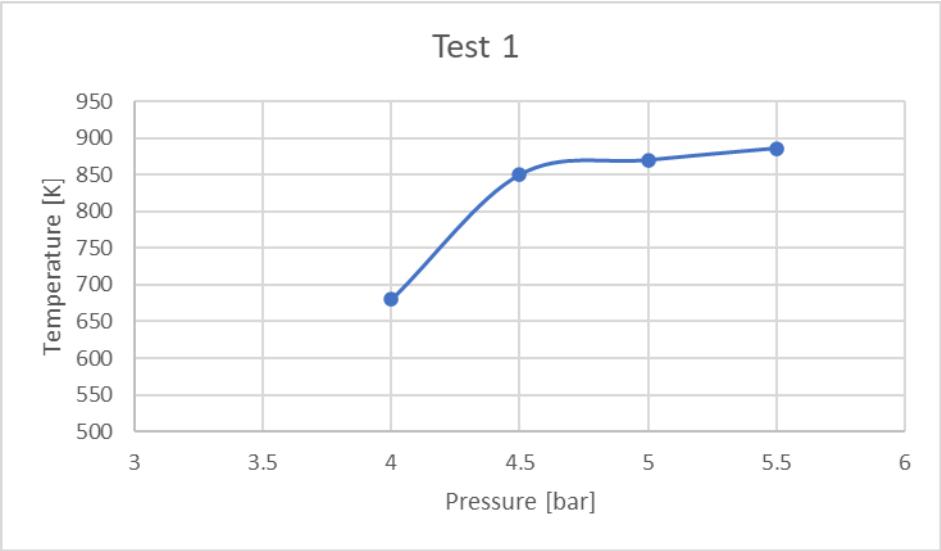

Figure 3.7: Temperatures recorded in the first test

The graph of *Figure 3.7* shows the temperatures recorded during the first test with NPR varying between 5 and 6.5 corresponding to a relative pressure between 4 and 5.5 bar, with a constant distance between the nozzle and the resonator equal to 10 mm. With the exception of the first value at a pressure of 4 bar, the other results are between 800 K and 900 K with an increasing trend which makes advisable to carry out tests with higher pressures.

Test 2

Nozzle diameter (d)	4 mm
Nozzle-resonator distance (s)	16 mm
Relative pressure	4 – 5,5 bar
s/d	4

Table 3.5: Second test data

With this value of nozzle-resonator distance, the maximum temperatures reached were recorded for the various relative pressure values.

Relative pressure [bar]	Temperature [K]
4	**355**
4,5	**511**
5	**846**
5,5	**952**

Table 3.6: Temperatures recorded for the second test

In the second test the maximum temperature peak is reached with a relative pressure of 5.5 bar or with NPR = 6.5. Comparing the previous test, for lower pressures the temperatures obtained are considerably lower, this means that there is a great distance from the "optimal" conditions for this nozzle-resonator gap.

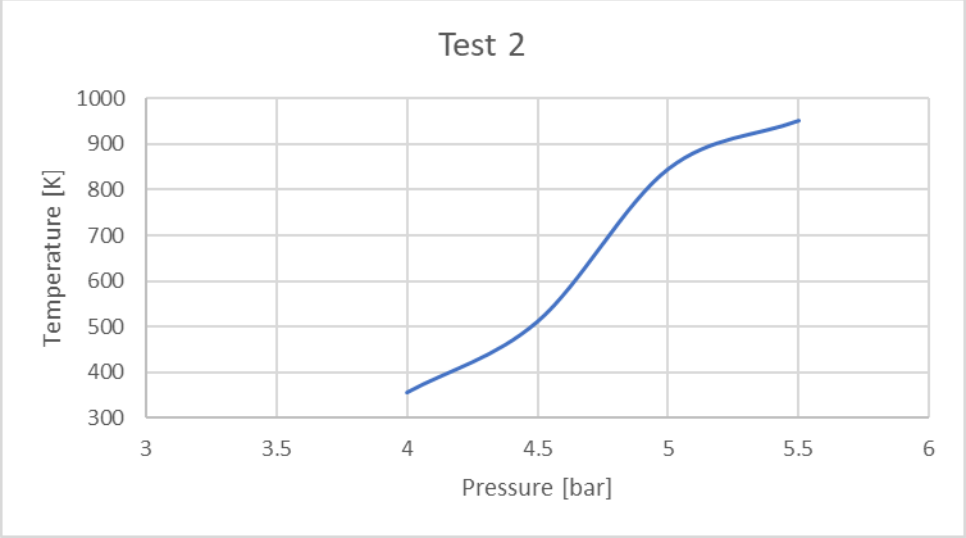

Figure 3.8: Temperature trend of test 2

Observing the results in this second test at a distance of 16 mm (*Table 3.6* and *Figure 3.8*), a temperature increase over 950 K is visible for high pressures. For the remaining values the temperatures are lower, this is more evident if the two curves are superimposed as shown in *Figure 3.9* below.

From this graph, a greater stability in temperatures clearly emerges for the first test at a distance of 10 mm, in fact the trend remains approximately constant starting from NPR 5.5, while for the distance of 16 mm the temperatures are lower except when the NPR is 6.5. However, in this second test the trend is very steep, a small variation in pressure during operation leads to a high lowering of temperatures causing possible problems in combustion; therefore this distance will be further analyzed in subsequent tests but from the first results it does not seem among those to be considered optimal.

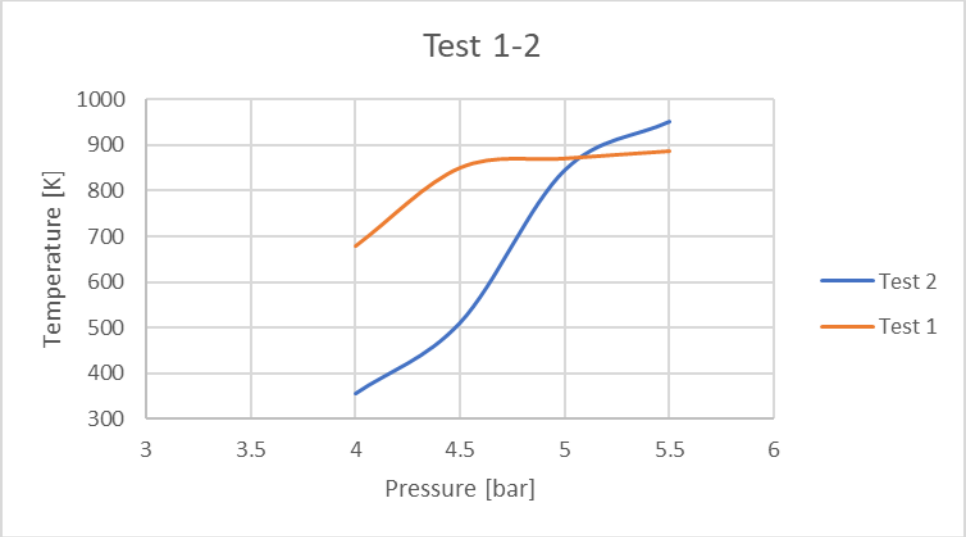

Figure 3.9: Test 1-2 comparison results

After the analysis of the temperatures reached, the graphs relating to the detected frequency peak are shown, this peak should occur at the fundamental frequency of the resonator, i.e. at about 1.9 KHz, in fact, as shown below, the value obtained experimentally follows the theoretical one.

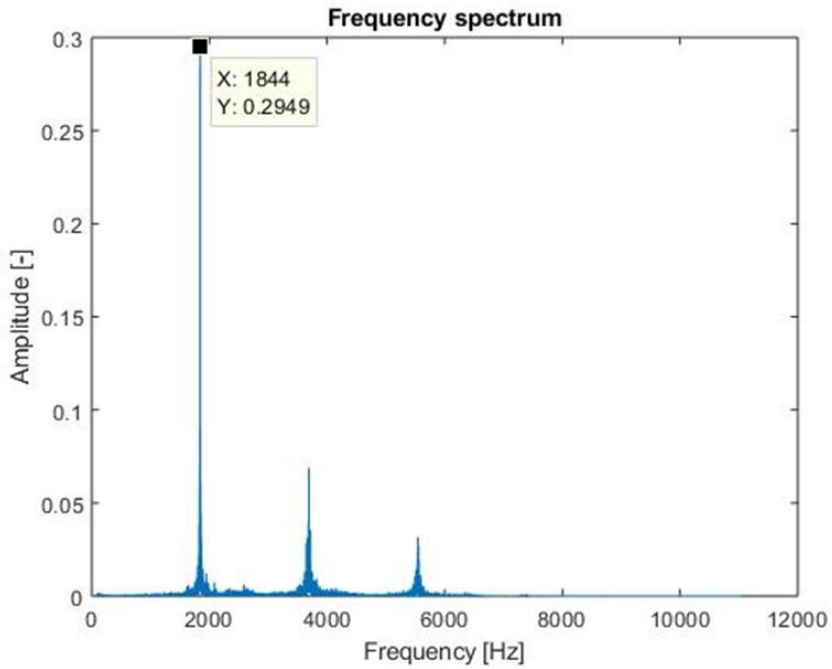

Figure 3.10: Frequency peak at 1844 Hz recorded during one of the tests

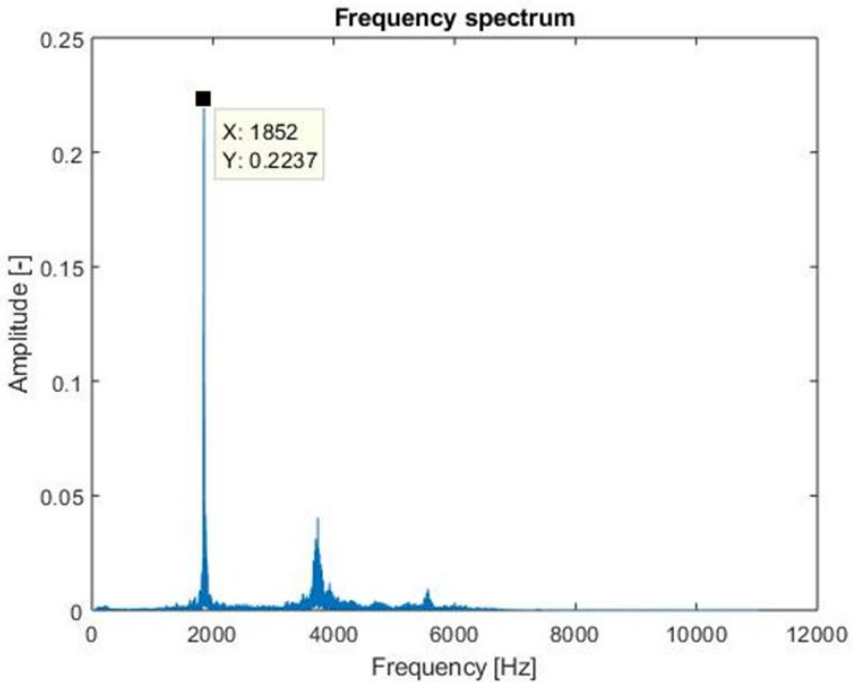

Figure 3.11: Frequency peak at 1852 Hz

Since the graphs show very similar values, only a few have been reported as an example, the complete results are instead included in *Table 3.7* and *graph 3.12*.

Summary table of test results 1-2

N°Test	Frequency [Hz]	Amplitude [-]
1	1998	0.03646
2	2027	0.7822
3	2009	0.6876
4	1791	0.2442
5	1844	0.2949
6	1852	0.2237
7	1777	0.3299
Average	1900	

Table 3.7: Frequencies and relative amplitudes recorded during the tests

As expected, the frequency peaks are not always found in the same point, there is a minimal discrepancy due to some factors, including the temperature increase in the resonator, an effect that will have considerable importance as visible in a subsequent test. However, the average value of the obtained results is 1.9 KHz in line with expectations.

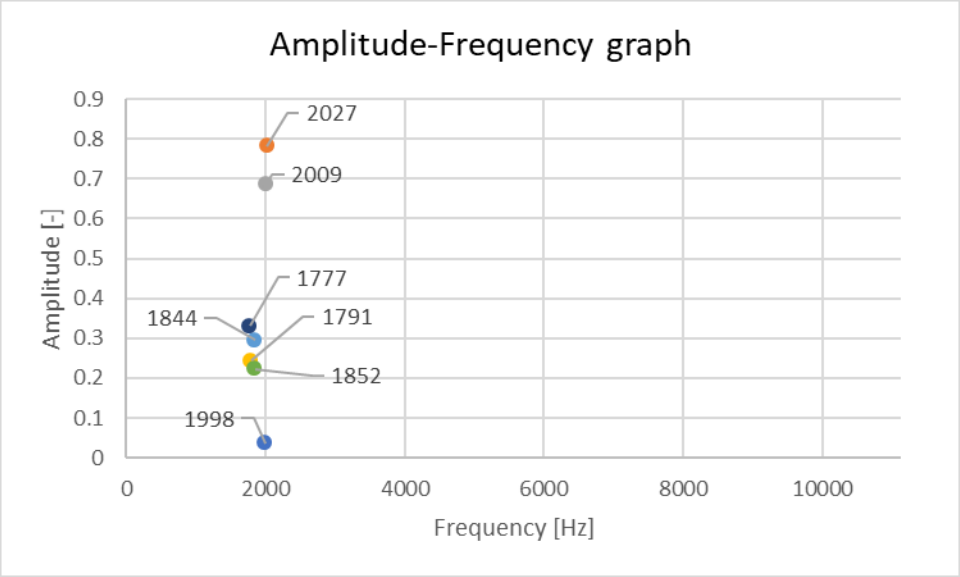

Figure 3.12: Amplitude-frequency graph of the tests carried out

3.3 Preliminary Conclusions

In this paragraph, after having carried out the first tests, some considerations are reported.

These results are in line with theoretical treatments and comparable to those obtained by others using similar parameters.

- From the theoretical point of view, it is likely that with increasing nozzle-resonator distance, the effects of greater heating are obtained at a higher pressure. In fact, as reported in the 1971 study by Phillips and Pavli, it is noted that as the nozzle-cavity distance increases, the maximum temperature peaks decrease, while keeping the nozzle pressure constant;[1] however considering the structure of an under-expanded jet flow composed of several cells that enclose the regions of instability, the resonance phenomenon occurs if the resonator inlet is placed inside these regions. With a greater distance it can be seen from the test carried out that the maximum temperature peak is obtained with a higher pressure value, because the structure of the under-expanded flow tends to move away from the nozzle as the pressure increases and consequently with a greater gap , in order for the resonator inlet to re-enter the region of instability, higher pressure values will be required as evidenced by the test at a distance of 16 mm in which the temperature peak of 952 K was reached with a pressure of 5.5 bar.

- The distance between the nozzle and the resonator is also similar with that used in the other experiments, in the same article by Phillips and Pavli the optimal considered distance is 11.4 mm,[1] in Haidn et al. article [3] this distance was of 12 mm while in that of Gupta et al. the distances vary from 10 to 15 mm,[4] therefore the two chosen distances (10 and 16 mm) are correct.

- A difference from Haidn et al.[3] experiment is the NPR value at which the temperature peak is obtained. In our tests this maximum is obtained at an NPR of 6.5 while in the previous article with NPR = 4,[3] however it must be considered that in our tests a vacuum chamber was not used to isolate the resonator and the geometry of the nozzle used in the other experiment is not clearly known, therefore it is not possible to make a 100% exact comparison.

- In the Haidn et al. experiment [3] the maximum temperature results were achieved at a S / d = 2.4, with a usable range to obtain the maximum temperatures between S / d = 2 and S / d = 4, therefore also for these parameters our choices are consistent.

- The tests carried out showed that the flow passing around the resonator had a significant impact on the temperature. To prevent this from lowering the values recorded by the thermocouple, a bulkhead was applied around it, in a similar way it was done in the experimental setup of Sarohia, Back, Roschke and Pathasarathy of 1976 in which a 33 cm diameter disc was applied around the resonator inlet in order to isolate the rear from the nozzle flow interference.[2]

To conclude, the results obtained in terms of temperature do not differ much from those of other experiments, for example in the study of Bauer, Pauw and Haidn using a stepped resonator contained in a vacuum chamber, an increase of more than 700 K was registered.[3] Gupta et al. reached 1060 K with an NPR of 6.25,[4] while in our tests a temperature of 952 K was recorded, an increase of about 660 K.

3.4 Second Test Campaign

This section initially describes the changes made to the experimental setup and then continues with the second test campaign with nozzle-resonator distance of 16 mm, 10 mm and 5 mm.

3.4.1 Improvements to the experimental setup

From previous experience some changes have been made to the experimental setup, in particular, the following changes are reported:

- Fixing thermocouple to the resonator with copper filament to prevent accidental disconnection during the various tests in order to obtain homogeneity in the results.

- Shielding the resonator from external interference as depicted in *Figure 3.13*.

- First tests carried out with a manometer connected to the compressed air line and verification of the effective pressure value with Arduino®.

- In order to verify operation for higher pressures, the last two tests were carried out with the manometer removed, simplifying the line in order to obtain pressure values up to 8.6 bar while previously it was not possible to rise above 5.5 bar.

Figure 3.13: Resonator-end at the maximum temperature reached during one of the tests, the protection from external interference is also visible

3.4.2 Tests Carried Out

The following tests 3 and 4 are repetitions of the previous ones in order to validate the conclusions drawn and verify the correct functioning of the changes made to the experimental setup.

Test 3

Nozzle diameter (d)	4 mm
Nozzle-resonator distance (s)	16 mm
Relative pressure	4 – 5,5 bar
s/d	4

Table 3.8: Third test data

With this value of the nozzle-resonator distance and for different pressure values, the maximum temperatures reached were recorded:

Pressure [bar]	Temperature [K]
4	**544**
4,5	**729**
5	**821**
5,5	**845**

Table 3.9: Results of the third test

From *Table 3.9*, the maximum temperature reached was 845 K, with a pressure of 5.5, i.e. NPR = 6.5. By comparing the result with the test carried out during the first campaign, a temperature difference of about 100 K is noted, the reason can be found in the new thermocouple position, since the surface of the resonator is small and the area subject to intense heating is even smaller, a minimal variation in the positioning of the thermocouple determines a strong variation in terms of the maximum temperature recorded.

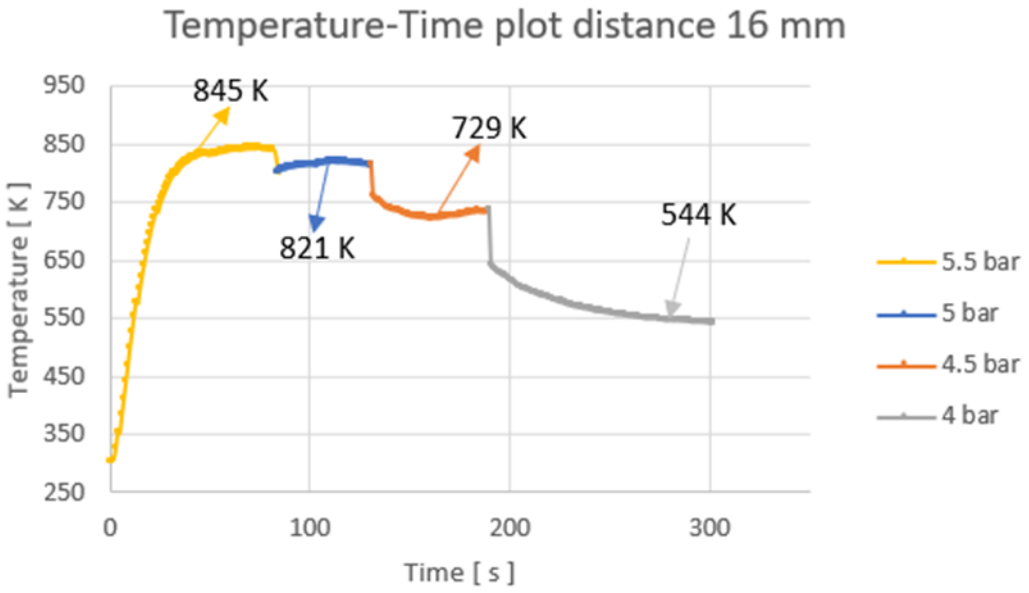

Figure 3.14: Temperature trend over time for various pressure values at a distance of 16 mm

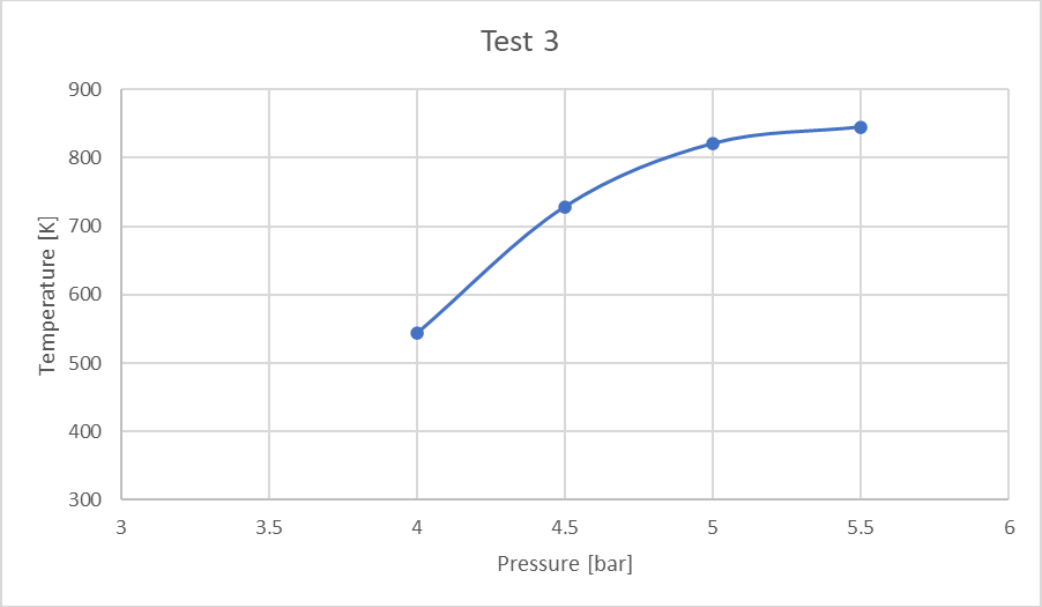

Figure 3.15: Temperature-pressure trend test 3, distance 16 mm

In this graph of *Figure 3.15* the temperature trend is very similar to the previous chart obtained in test 2 relative to the same distance of 16 mm, that is a steep growth with the increase in pressure which confirms once again the conclusions drawn in the previous attempt.

Following the previous diagram, some FFT graphs are shown, they are obtained at a distance of 16 mm for different NPR values.

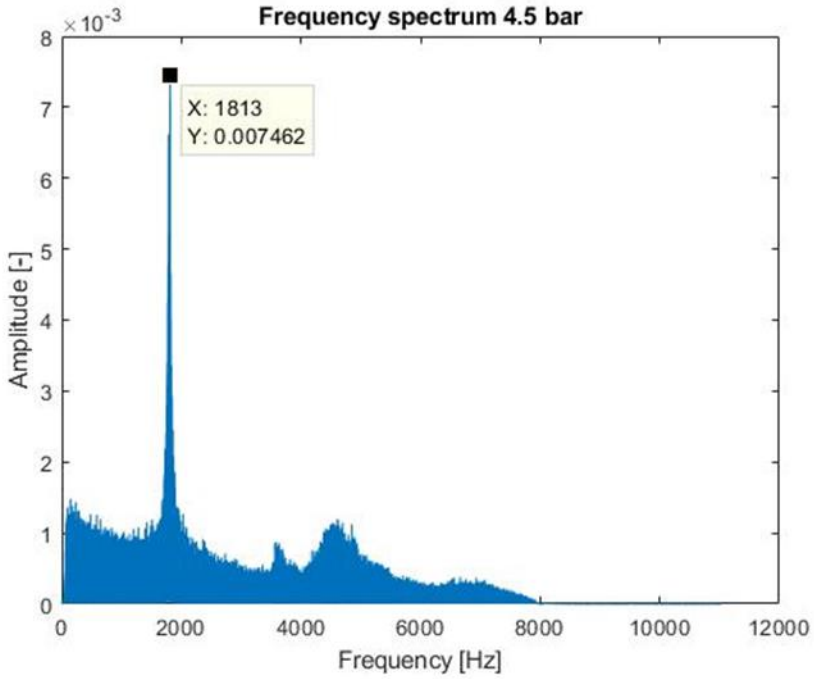

Figure 3.16: FFT graph at a relative pressure of 4.5 bar

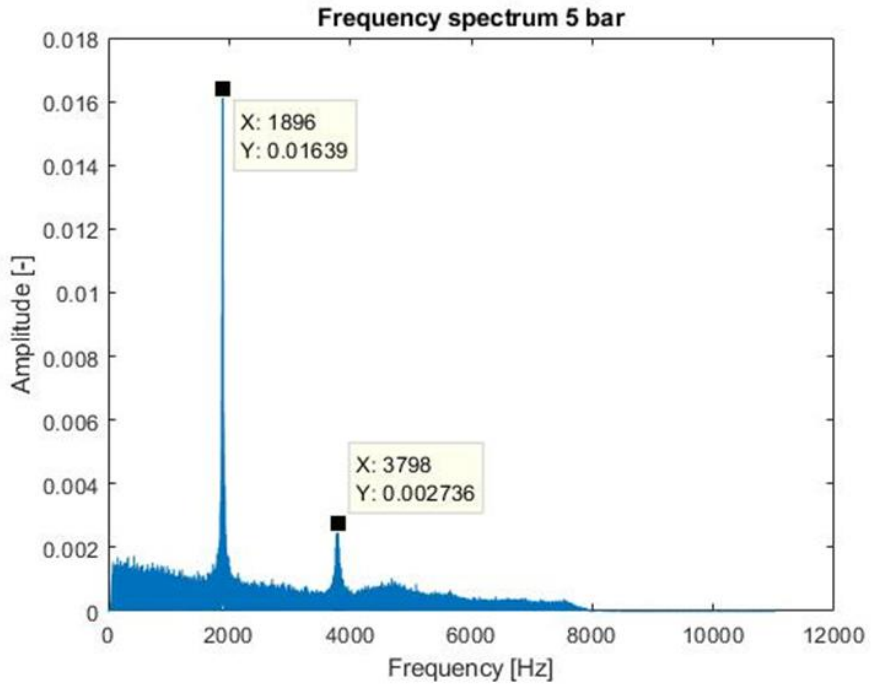

Figure 3.17: FFT graph at a relative pressure of 5 bar

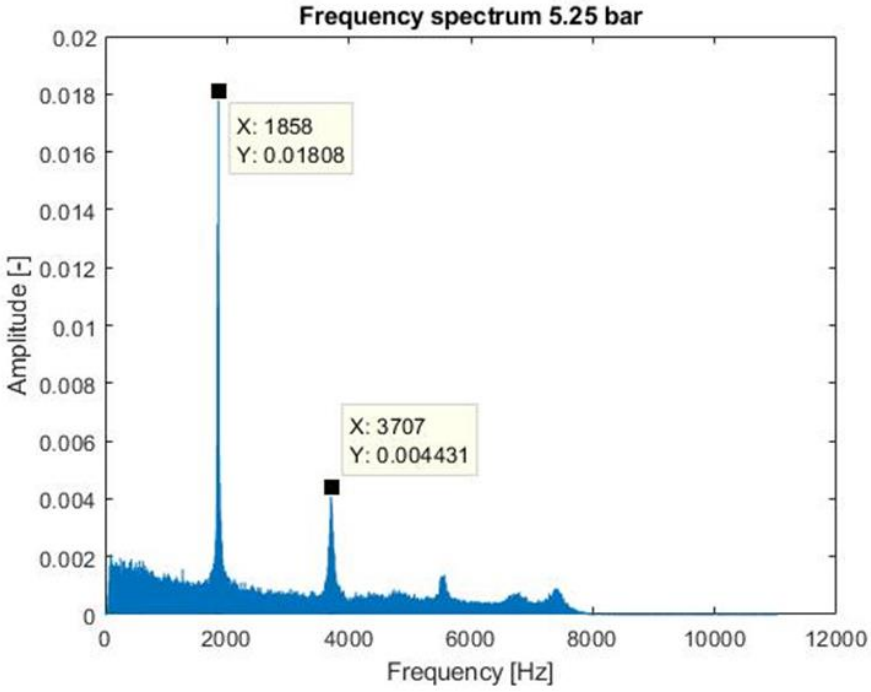

Figure 3.18: FFT graph at a relative pressure of 5.25 bar

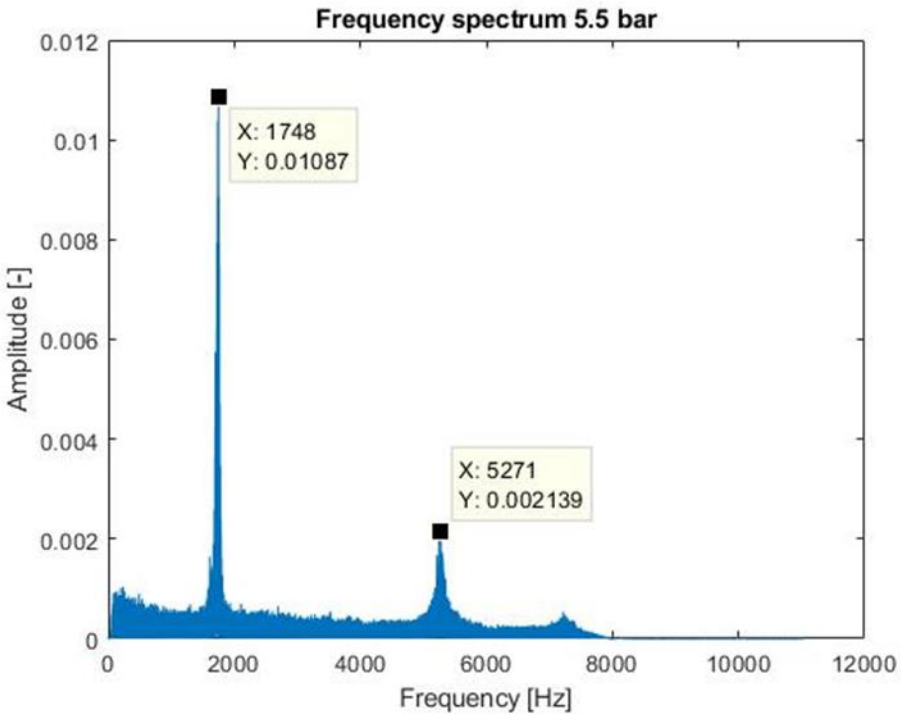

Figure 3.19: FFT graph at a relative pressure of 5.5 bar

In these graphs it can be seen that with the increase in relative pressure up to NPR = 6, there is an increase in the frequency peak up to 1896 Hz and then slightly decreases up to 1748 Hz with an NPR = 6.5. The second frequency peak of about 3700 Hz is visible up to 5.25 bar; in the last case with a pressure of 5.5 bar it is not visible while a peak appears at a frequency of 5271 Hz.

Test 4

Nozzle diameter (d)	4 mm
Nozzle-resonator distance (s)	10 mm
Relative pressure	4,5 – 5,5 bar
s/d	2.5

Table 3.10: Fourth test data

With this value of the nozzle-resonator distance and for different pressure values, the maximum temperatures reached were recorded.

Pressure [bar]	Temperature [K]
4,5	**859**
5	**889**
5,5	**921**

Table 3.11: Fourth test results

From *Table 3.11*, the maximum temperature recorded was 921 K with a relative pressure of 5.5 bar, i.e. NPR = 6.5, even for greater distances such as the 16 mm of the previous test, the maximum temperature was detected with this pressure value. However, this gap between nozzle-resonator is more efficient than the previous one because the temperatures obtained are higher.

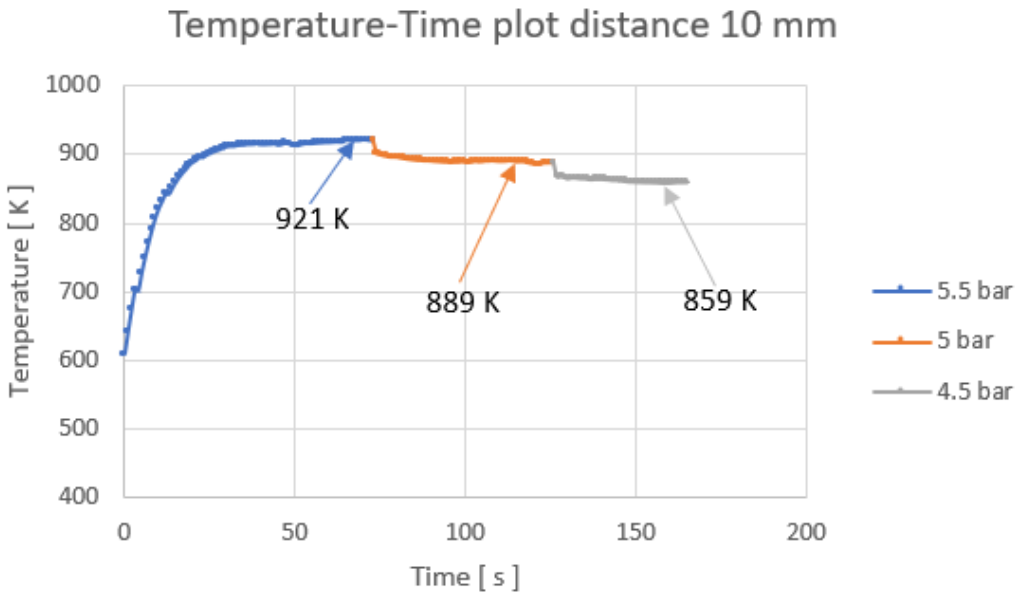

Figure 3.20: Temperature trend over time during the fourth test at a distance of 10 mm

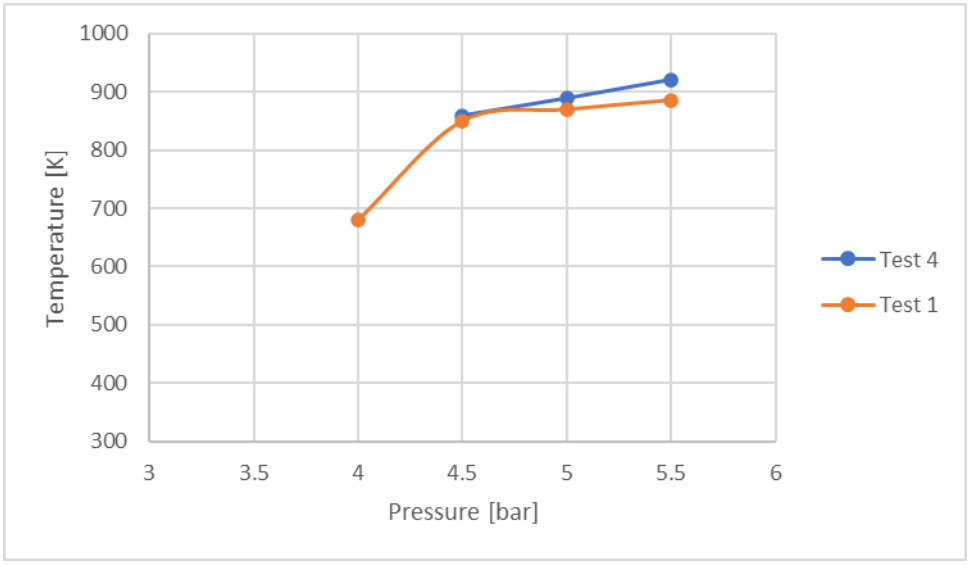

Figure 3.21: Comparison of test 4 and test 1 results at the same distance of 10 mm

As shown by the graph in *Figure 3.21*, the temperature trend is increasing with the pressures, the blue curve indicates test 4 just carried out while the orange curve indicates the previous test 1 at the same distance. Leaving aside small

discrepancies due to innumerable factors such as the displacement of the thermocouple and the variation of climatic conditions, the two behaviors are almost superimposable and undergo minimal variations with the pressure; this allows us to consider this distance as the best between the two tested until now.

As usual, the signal recorded during the tests is analyzed in order to obtain the FFT graphs. *Figure 3.22* shows the first graph obtained in the early stages of the analysis. In fact, it reports the signal recorded by the microphone positioned between the nozzle outlet and the cavity inlet.

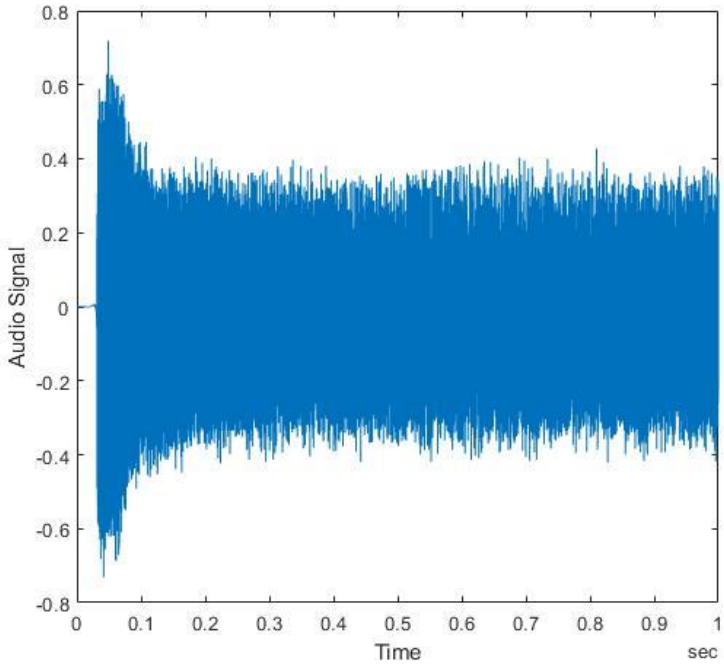

Figure 3.22: Graph of the signal over time recorded during test 4 with relative pressure 4.5 bar

Below are some FFT graphs obtained at various pressures starting from that with relative pressure 4.5 bar equivalent to NPR = 5.5

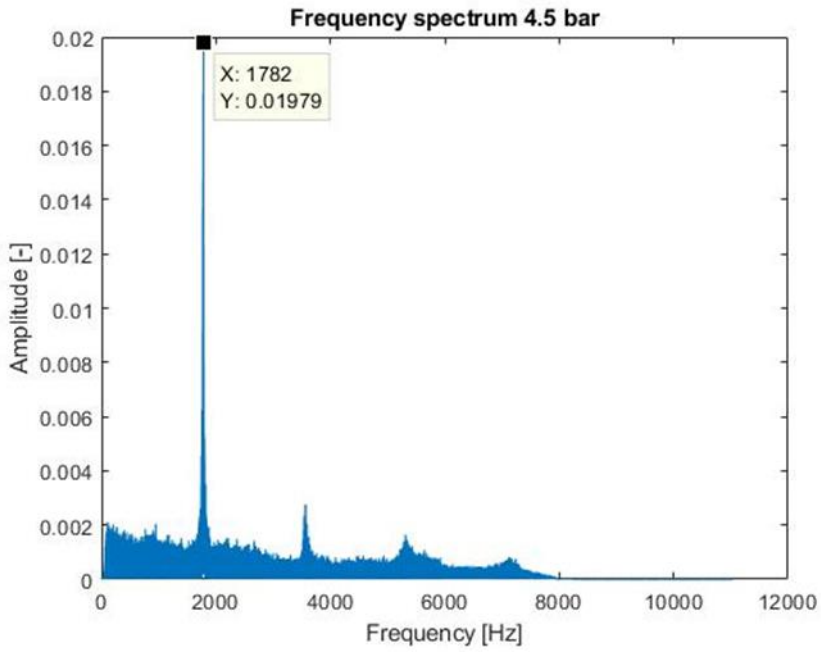

Figure 3.23: Test 4 frequency spectrum with a relative pressure of 4.5 bar

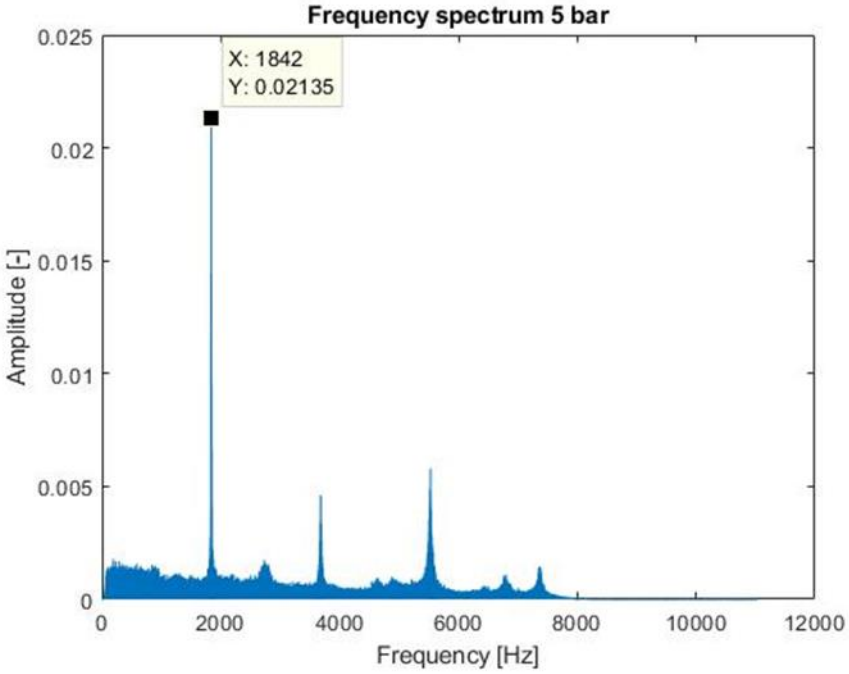

Figure 3.24: Test 4 frequency spectrum with a relative pressure of 5.5 bar

Analyzing all the recorded signals, the peak frequency is between 1782 Hz and 1907 Hz, this frequency increases with increasing pressure values (i.e. NPR) and temperatures since the maximum value was recorded at 5.5 bar.

In fact the frequency is linked to the speed of sound, which in turn depends on the temperature, because in the formula the speed of sound is in the numerator, an

increase in it determines in turn an increase in the frequency as shown in the previous graphs of *Figures 3.23* and *3.24*. The secondary peaks (3.8 KHz and 5.8 KHz) are also increasing, in particular with 5.5 bar the amplitudes of both are comparable.

Test 5

Nozzle diameter (d)	4 mm
Nozzle-resonator distance (s)	5 mm
Relative pressure	4,5 – 5,5 bar
s/d	1.25

Table 3.12: Fifth test data

With this value of the nozzle-resonator distance and for different pressure values, the maximum temperatures reached were recorded.

Pressure [bar]	Temperature [K]
4,5	**476**
5	**530**
5,5	**396**

Table 3.13: Fifth test results, pressures and temperatures

The performances obtained in this test are not optimal, in fact the characteristic "whistle" typical of the resonance was not detected, probably the distance between the nozzle and the resonator is too small. This is also evident from the lower temperatures reached (*Table 3.13*).

In the following graph of *Figure 3.25* it can be seen that the maximum temperature reached was 530 K at a pressure of 5 bars, i.e. with NPR = 6, while lower values were recorded both with a higher pressure equal to 5.5 bar and a lower one of 4.5 bar. This trend did not occur in the other tests with greater distances.

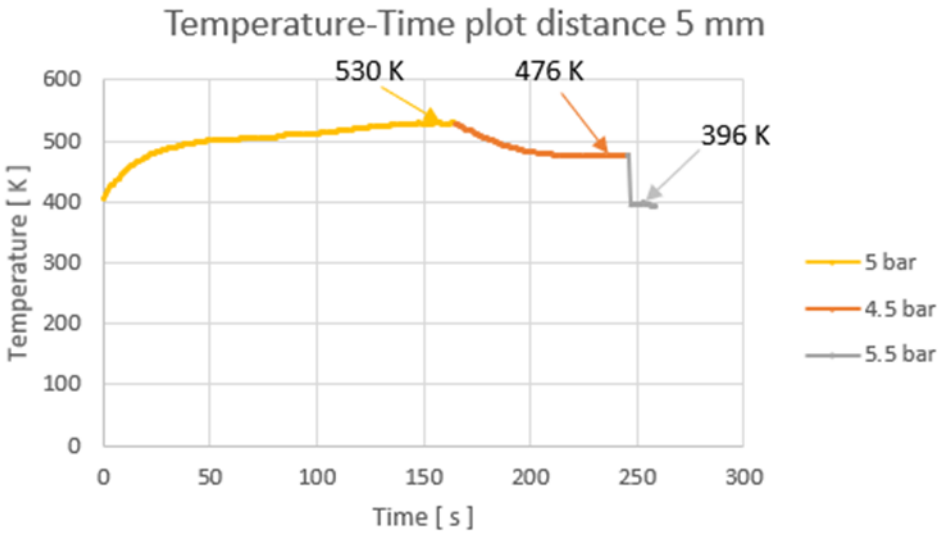

Figure 3.25: Temperatures recorded as a function of time during the fifth test

The frequency spectrum, obtained by analyzing the signal, is shown in *Figure 3.26*. As you can see from the graph, the resonator characteristic frequency is not present, the frequency peaks vary from 634 Hz of the first attempt with 4 bar to 762 Hz of the attempt with 5 bar, the trend is increasing with increasing relative pressure and temperature, the heating is however minimal, therefore this distance must be discarded because it is too small.

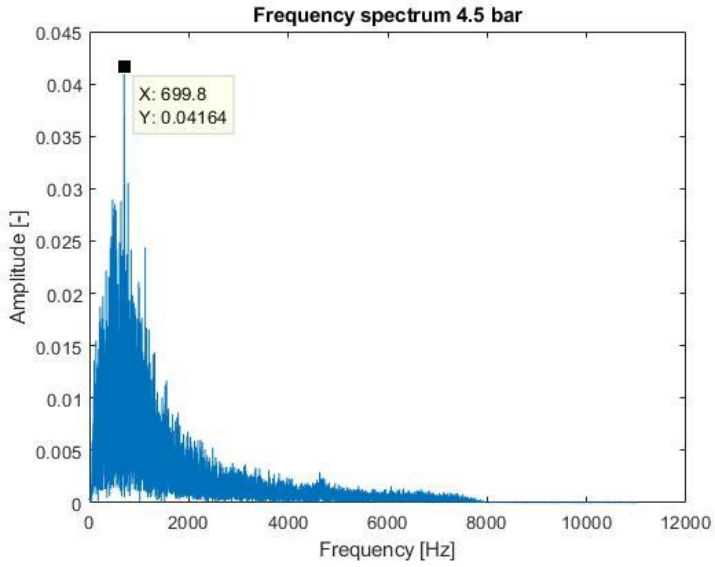

Figure 3.26: Test 5 FFT graph with relative pressure of 4.5 bar

Test 6 without Manometer

In order to reach higher nozzle inlet pressures, it was decided to remove the pressure gauge from the compressed air line to carry out some tests.

Nozzle diameter (d)	4 mm
Nozzle-resonator distance (s)	16 mm
Relative pressure	7 / 8.3 bar
s/d	4

Table 3.14: Sixth test data without manometer

With this value of the nozzle-resonator distance and for different relative pressures, the maximum temperatures reached were recorded.

Pressure [bar]	Temperature [K]
7	**914.5**
8.3	**913.5**

Table 3.15: Sixth test results

The following graph in *Figure 3.27* shows the temperature trends over time and the maximum values reached for the two pressure values also reported in *Table 3.15*, the difference is minimal but the greater heating was obtained with the lower relative value, equal to 7 bar (NPR = 8), which corresponds to a slight increase in temperature.

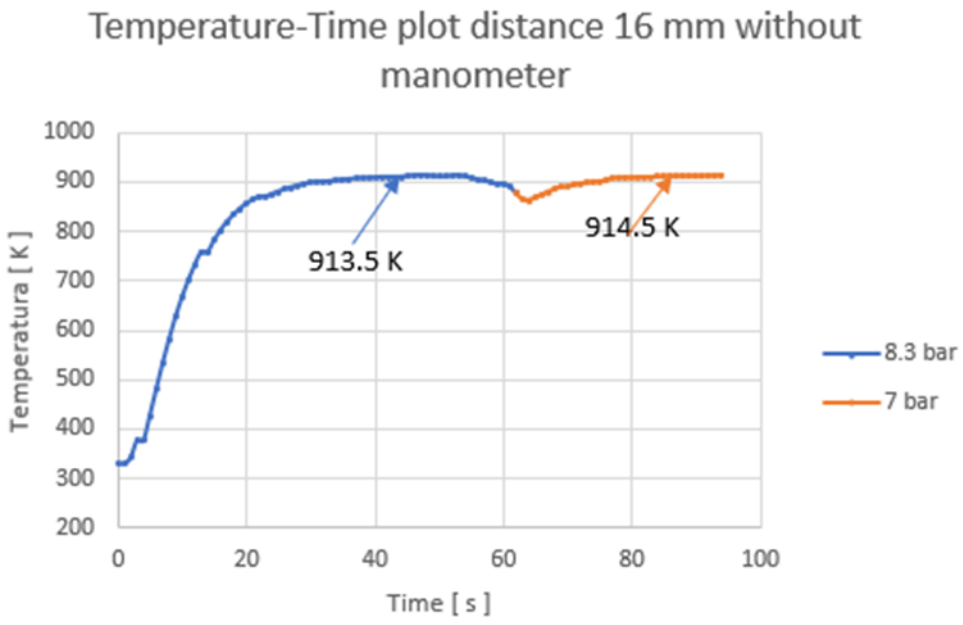

Figure 3.27: Temperature trend over time, test 6

A summary graph in *Figure 3.28* shows the temperature trends over time: in the first part the trend is increasing with pressures that increase up to 5.5 bar while in the second part the temperature increases as the pressure decreases. It is also possible that the optimal value of pressure and therefore of NPR for that nozzle-resonator distance lies in the still unexplored range.

A first hypothesis that justifies this behavior is the fact that with a greater gap between the nozzle and the resonator, the pressures must be greater so that the area of instability (first cell) of the under-expanded jet structure is positioned in front of the cavity entrance.

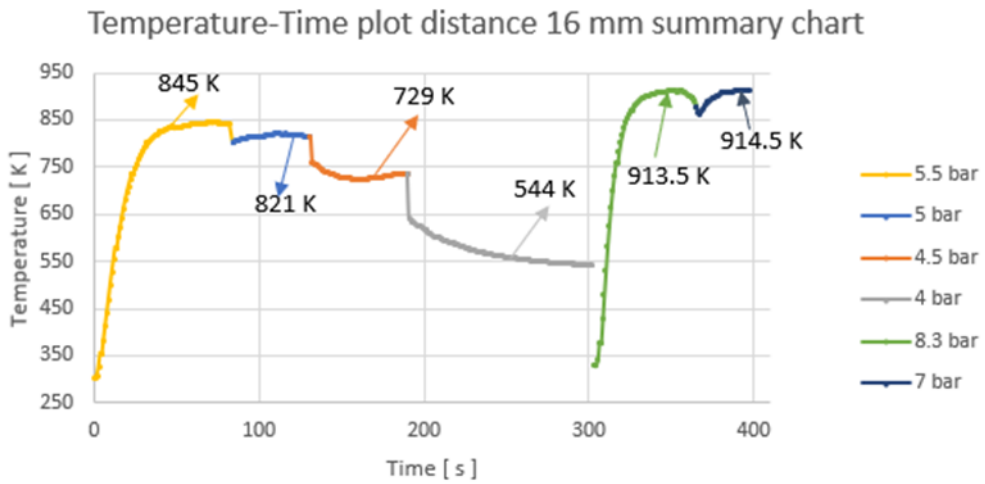

Figure 3.28: Summary graph of the temperature trend over time at a distance of 16 mm

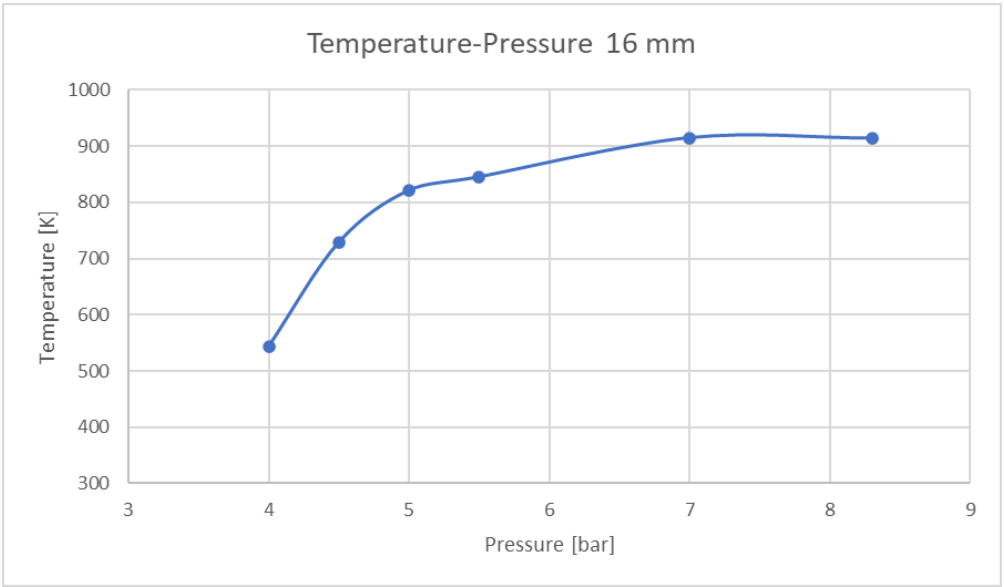

Figure 3.29: Summary temperature-pressure graph for 16 mm distance

To conclude this second test campaign, the graph in *Figure 3.29* shows the trend of temperatures as a function of pressure for a distance of 16 mm. The first part, as mentioned above, has a very steep trend when compared, for example, with the results obtained at a distance of 10 mm, while for relative pressures above 5.5 bar the trend seems less variable with small fluctuations in the region of 900 K.

3.5 New Test Session, Third Campaign

In this new session, tests were carried out at distances of 12 and 10 mm for different pressure values. In particular, the test at a distance of 12 mm was repeated by varying the position of the thermocouple in order to evaluate its impact on the results.

Test 7

Nozzle diameter (d)	4 mm
Nozzle-resonator distance (s)	12 mm
Relative pressure	4- 8.6 bar
s/d	3

Table 3.16: Technical data for test 7

With this value of the nozzle-resonator distance and for different relative pressures, the maximum temperatures reached were recorded.

Pressure [bar]	Temperature [K]
4	587
4.5	700
5	788
6	806
7	811
8.5	869
8.7-8.5	939

Table 3.17: Temperatures and pressures recorded during test 7

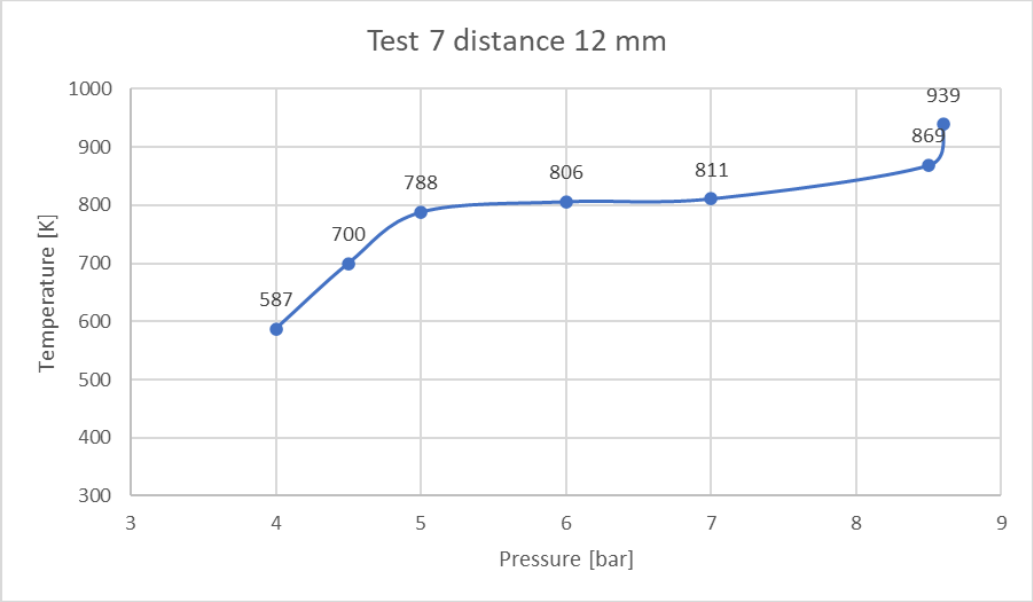

Figure 3.30: Graph of temperature as a function of relative pressure for test 7 at a distance of 12 mm

Observing the graph in *Figure 3.30*, a large area can be seen in which the temperature variation is minimal, in particular from the relative pressure of 5 bar to 8.5 bar corresponding to NPR = 6 - 9.5. In this range, the temperature difference is only of 81 K.

From the analysis of the signals over time through a matlab program, the FFT graphs are shown with an indication of the fundamental frequency for some relative pressure values.

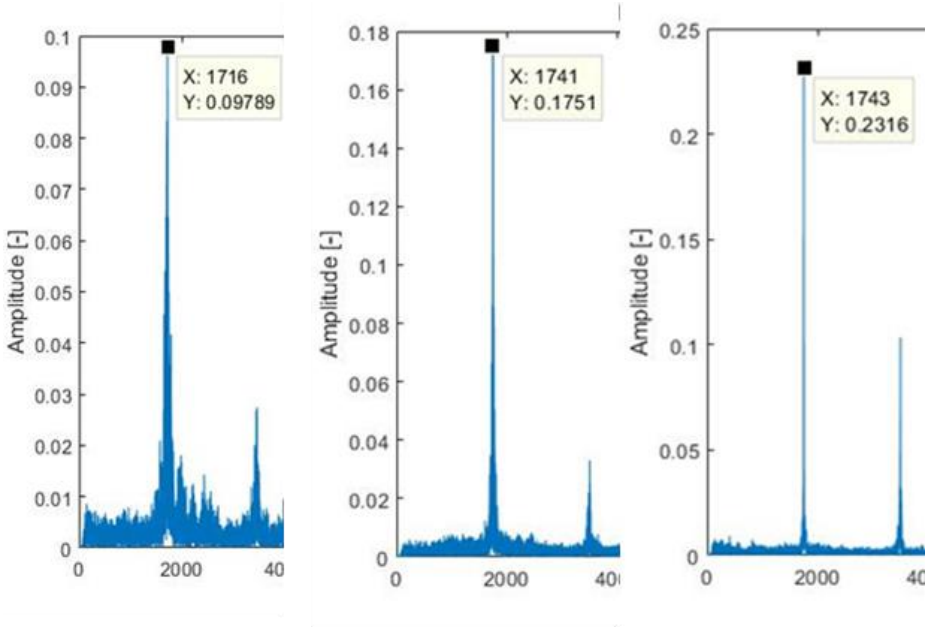

Figure 3.31: FFT graphs of test 7, from left to right frequency spectrum at a relative pressure of 4, 4.5 and 5 bar

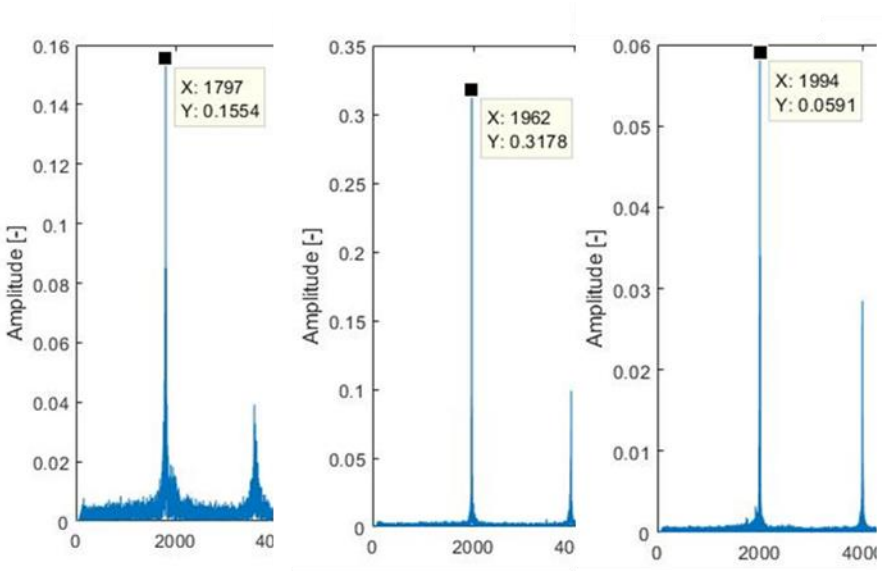

Figure 3.32: FFT graphs of test 7, from left to right frequency spectrum at a relative pressure of 7, 8.5 and 8.6 bar

As can be seen from the FFT graphs of *Figure 3.31* and *3.32*, starting from the first relative pressure value of 4 bar, i.e. NPR = 5, the frequency tends to rise with increasing temperature. In particular, it starts from a frequency peak of 1716 Hz at 4 bar up to 1994 Hz with a pressure of 8.6 bar which corresponds to the maximum temperature value recorded for this test.

The same test was repeated by changing the thermocouple location in order to evaluate the influence of its positioning on the recorded temperatures and the new results are shown in *Table 3.18* below.

Pressure [bar]	Temperature [K]
4	783
6	916
7	940
8.2	1006
8.3	992

Table 3.18: Temperatures recorded with the new thermocouple position at a distance of 12 mm

The comparison with the previous results shows an increase in temperatures, it is likely that the thermocouple new position is in a warmer area than the previous

one, which makes evident the strong effect of the positioning on the results in terms of temperature. To conclude, during this test with a pressure of 8.2 bar, that is NPR = 9.2, 1000 K was exceeded, reaching 1006 K.

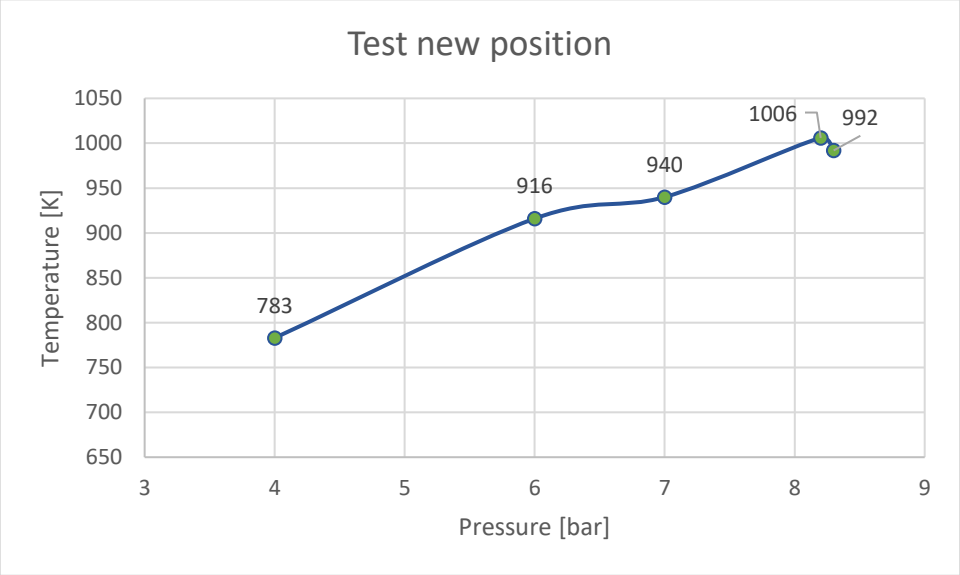

Figure 3.33: Temperature-relative pressure graph, test results with new thermocouple position

The graph in *Figure 3.33* shows the results of the test carried out with the new thermocouple position. Excluding the first result at the relative pressure of 4 bar, for values between 6 bar and 8.3 bar the temperatures fluctuate in less than 100 K, even the 12 mm distance is to be considered optimal because it shows minimal variations as the relative pressure varies or the NPR.

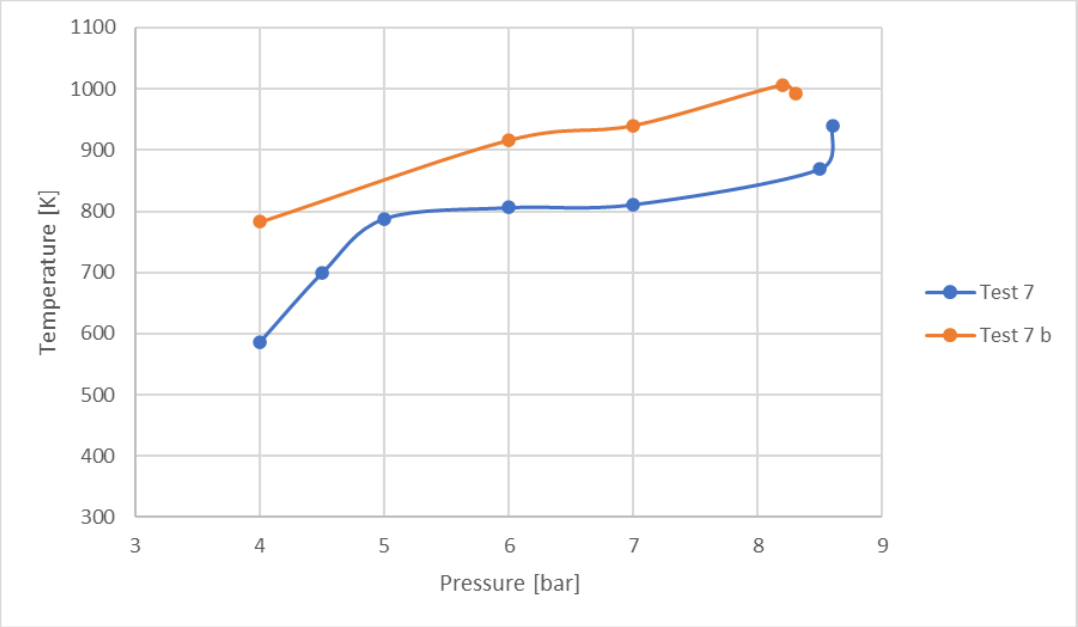

Figure 3.34: Comparison between the first test at a distance of 12 mm and the next with the new thermocouple positioning

In the graph of *Figure 3.34* a comparison is made between the first test (test 7) at a distance of 12 mm and the second one (test 7b) at the same distance with a new thermocouple positioning. The trend of the two tests is very similar, however it is clear that the new position of the thermocouple is in an area subject to greater heating.

To complete this new test, some FFT graphs are shown.

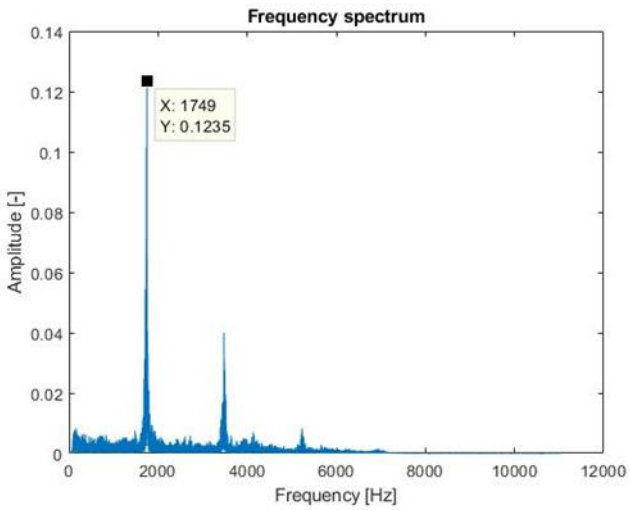

Figure 3.35: Frequency spectrum at a relative pressure of 4 bar

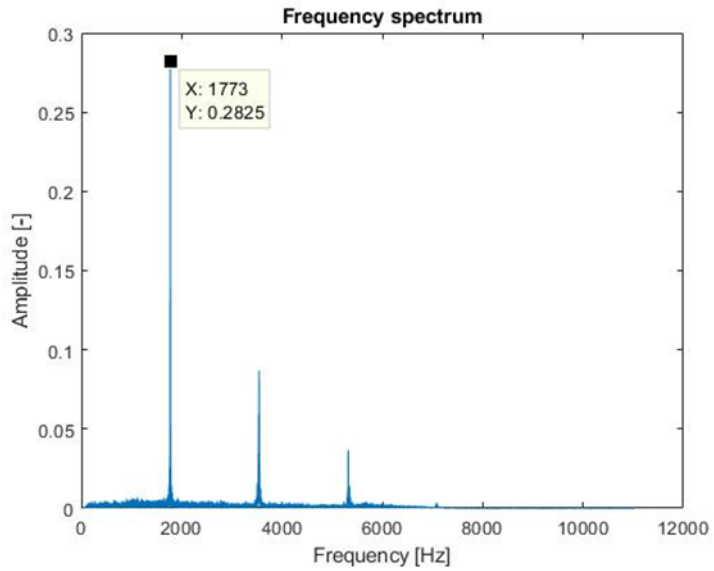

Figure 3.36: Frequency spectrum at a relative pressure of 6 bar

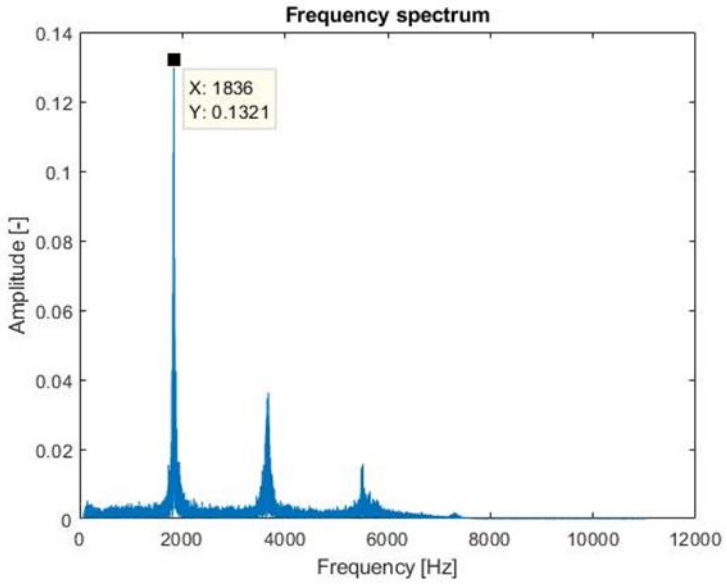

Figure 3.37: Frequency spectrum at a relative pressure of 7 bar

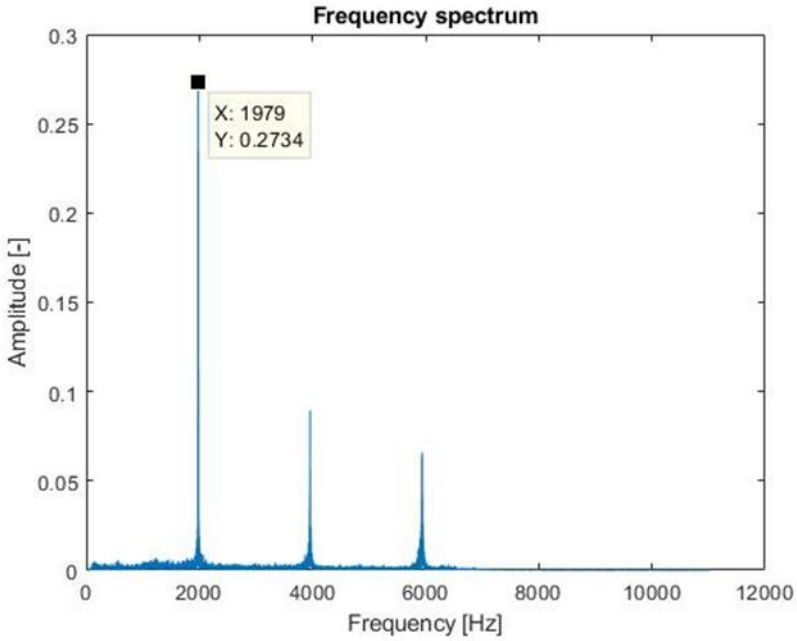

Figure 3.38: Frequency spectrum at a relative pressure of 8.2 bar

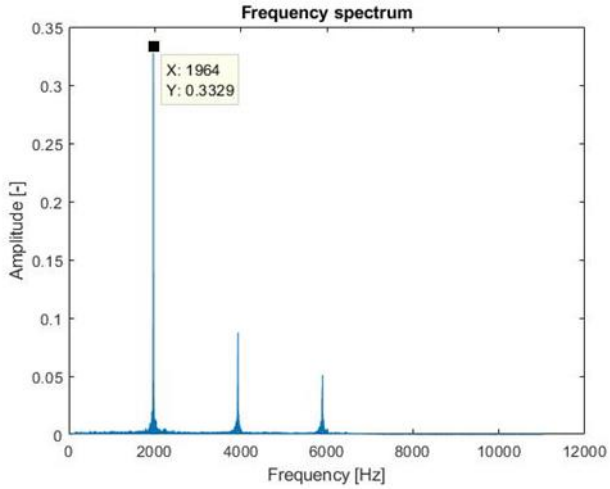

Figure 3.39: Frequency spectrum at a relative pressure of 8.3 bar

Also in this new test (test 7b) the increase in frequency with temperature emerges from the FFT graphs starting from *Figure 3.35* to *Figure 3.39*. In this series it is more evident, in fact there is an increasing trend up to 8.2 bar, where the maximum temperature is reached, after which for a higher-pressure value, i.e. 8.3 bar, the temperature drops slightly as well as the frequency, whose value (1964 Hz from *Figure 3.39*) is between that at 8.2 bar and 7 bar respectively 1979 Hz and 1836 Hz.

Additional Test Results

An additional test at the same distance of 12 mm was carried out. As in the previous one, the pressure gauge has been removed from the compressed air line in order to simplify it and reach a higher-pressure value, finally, the results achieved are reported in the following *Table 3.19*.

Pressure [bar]	Temperature [K]
8.5	**961**

Table 3.19: Additional test results at a distance of 12 mm

Figure 3.40 shows the temperature trend over time recorded during the additional test carried out at a distance of 12 mm with a relative pressure of 8.5 bar. After an initial transient characterized by a rapid increase in temperature, the trend remains almost unchanged over time, in fact it remains at the maximum temperature for about 30 seconds, recording a maximum value of 961 K.

Comparing with the results of the previous test 7b, this temperature value is perfectly in line with the decreasing trend recorded starting from 8.3 bar where the temperature dropped slightly from the peak of 1006 K obtained with a relative pressure of 8.2 bar up to 992 K.

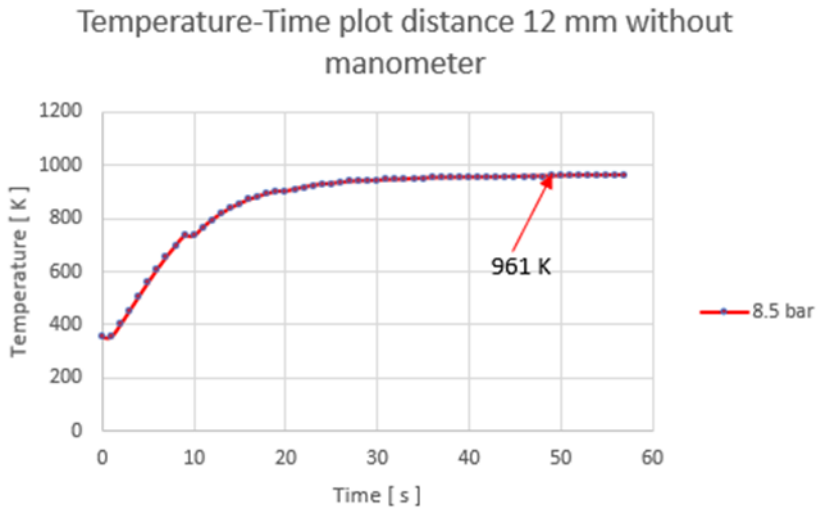

Figure 3.40: Temperature trend over time at the cavity bottom

Figure 3.41 below shows the relative frequency spectrum. This graph confirms the trend of the frequency peak, that is the increase of this one with higher pressures

and temperatures, in fact for a pressure of 8.5 bar, 961 K are reached and a clear peak is visible at a value of 1964 Hz.

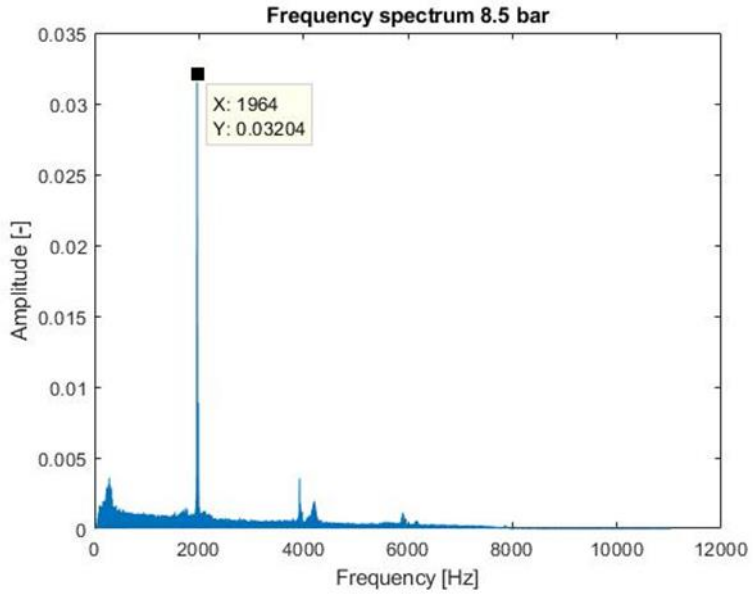

Figure 3.41: FFT graph of the supplementary test at a relative pressure of 8.5 bar

Test 8

Nozzle diameter (d)	4 mm
Nozzle-resonator distance (s)	10 mm
Relative pressure	5.5 – 9 bar
s/d	2.5

Table 3.20: technical data for test 8

With this nozzle-resonator distance and for different pressure values, the maximum temperatures reached during the tests were reported.

Pressure [bar]	Temperature [K]
5.5	871
6	885
6.5	908
7	930
7.5	936
8	937
8.5	936
9	924

Table 3.21: temperature and pressure results for test 8 at a distance of 10 mm

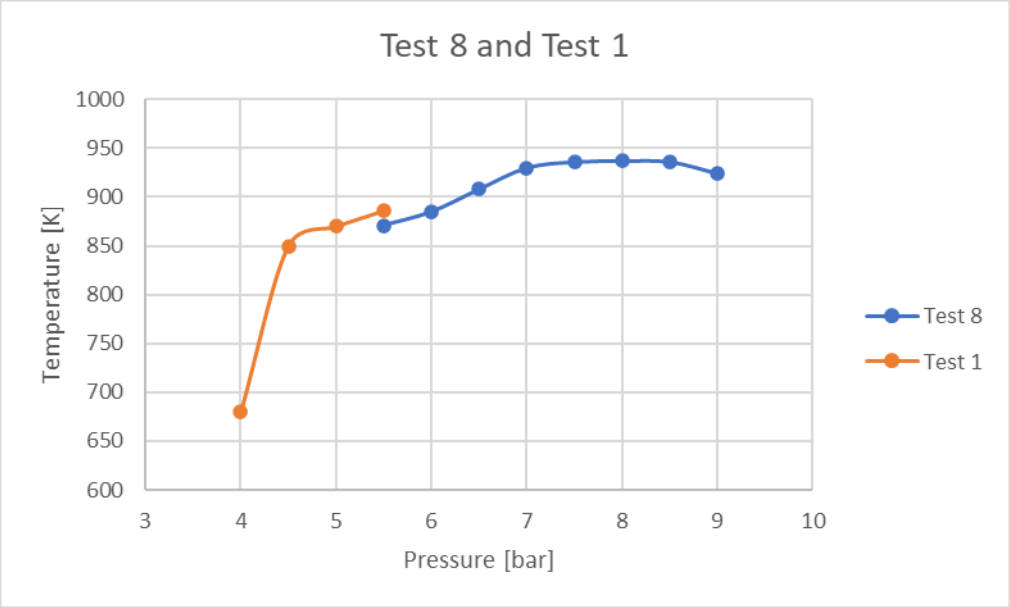

Figure 3.42: Graph of temperature-relative pressure test 8

The graph in *Figure 3.42* shows the results of test 8 performed with a distance between nozzle and resonator equal to 10 mm. As highlighted in the first tests carried out, this gap is to be considered one of the most optimal, in fact for NPRs between 7 and 10 the temperature at the cavity bottom undergoes minimal variations for different relative pressure values, which gives the system greater operating stability. For the sake of completeness, the temperature trend of test 1 (orange curve) is shown, whose behavior matches very well with the trend described by test 8, furthermore by combining the data it is possible to deduce that for NPR between 5.5 and 10 the maximum temperature variation is less than 100 K.

Frequency spectra for the different relative pressure values:

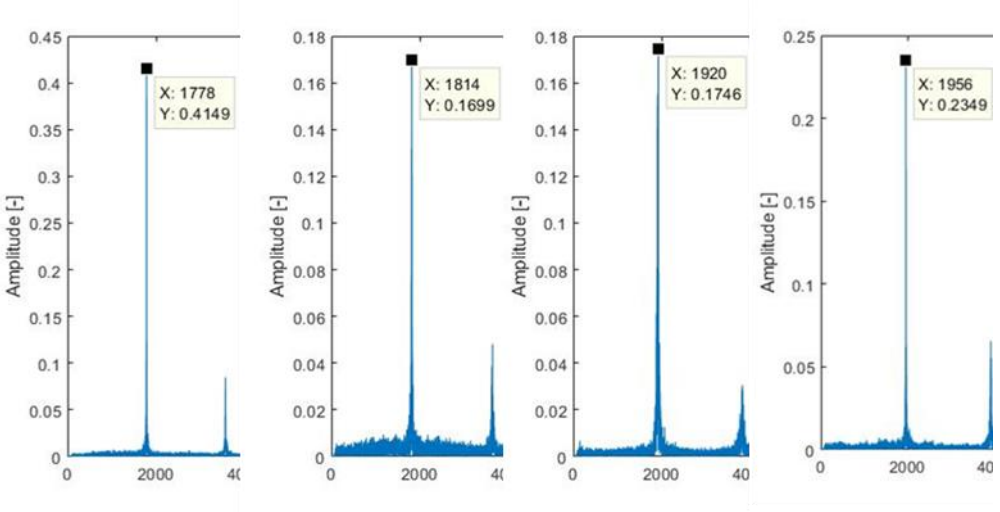

Figure 3.43: Different FFT graphs, from left to right, frequency peaks at a relative pressure of 5.5, 6, 6.5 and 7 bar

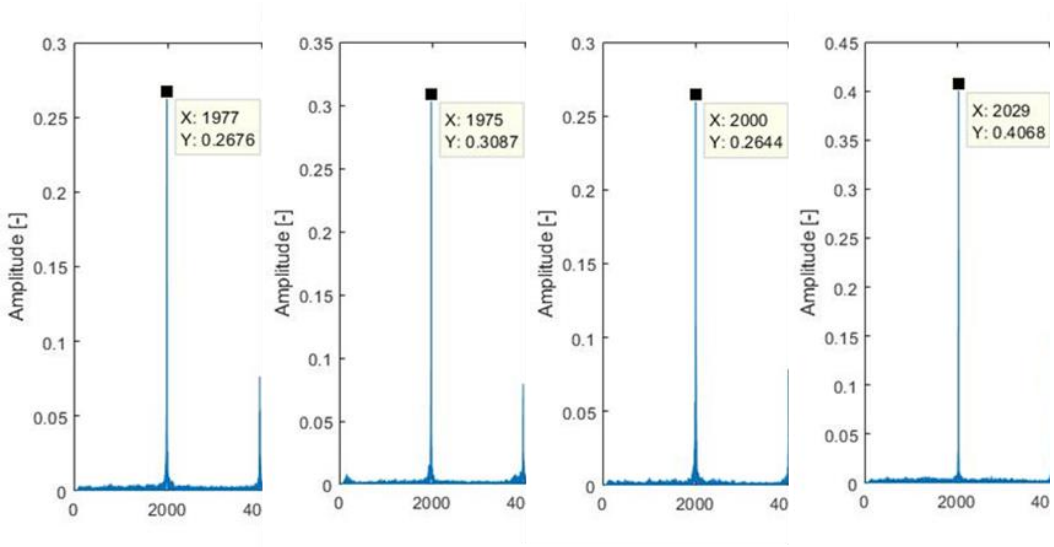

Figure 3.44: FFT graphs test 8, from left to right, frequency peaks at a relative pressure of 7.5, 8, 8.5 and 9 bar

From both the previous images (*Figures 3.43* and *3.44*) it is possible to follow the trend of the frequency peaks with the temperature and relative pressure values. This test was carried out with a greater range of nozzle pressure ratio, in fact they are between 5.5 bar and 9 bar.

At the end of this third campaign (tests 7 and 8) a summary table follows which shows the frequencies recorded during the tests with different NPRs.

DISTANCE	RELATIVE PRESSURE [BAR]	FREQUENCY [HZ]	AMPLITUDE [-]
10 MM	5.5	1778	0.4149
	6	1814	0.1699
	6.5	1920	0.1746
	7	1956	0.2349
	7.5	1977	0.2676
	7.7	2029	0.2752
	8	1975	0.3087
	8.3	2059	0.3607
	8.4	2050	0.4251
	8.5	2050	0.4251
		2000	0.2644
	9	2029	0.4068
		Test average 1969.75	
12 MM	4	1716	0.0979
		1743	0.1235
	4.5	1741	0.1751
	5	1743	0.2316
	6	1736	0.2724
		1773	0.2825
	7	1797	0.1554
		1836	0.1321
	8.2	1979	0.2734
	8.3	1964	0.3329
	8,5	1962	0.3178
	8.6	1994	0.0591
		Test average 1832	
AVERAGE		1901	

Table 3.22: Summary diagram of frequency- relative pressures of test 7 and 8

The following graph (*Figure 3.45*) shows the frequencies of the tests carried out, with an average value of 1,901 KHz they are around of the resonator characteristic frequency of about 1.9 KHz.

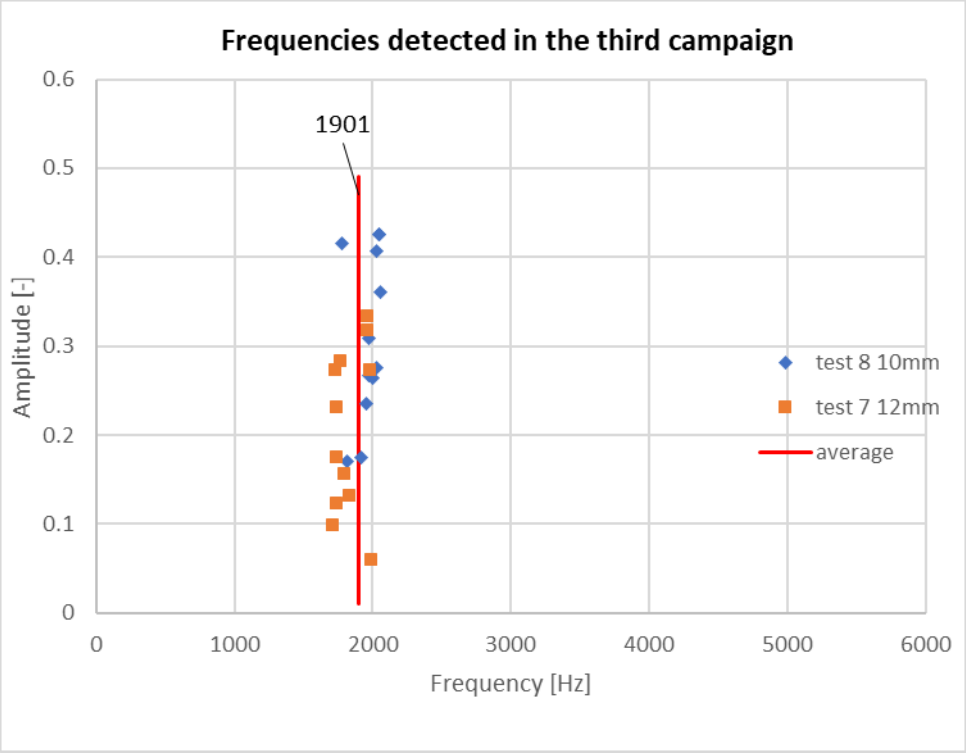

Figure 3.45: Frequency summary graph of Table 3.22

Chapter 4

Conclusions

In this final chapter, results obtained during the tests are highlighted in the first section together with the observations. A brief discussion follows on possible future developments and studies to be undertaken to continue the work carried out until now.

4.1 Conical Resonator Tests Conclusions

After the three experimental campaigns, it is possible to compare the results and draw conclusions.

The following table gives an overview of the tests performed, the yellow boxes indicate the tests carried out, while the red ones indicate the point where the maximum temperature was reached for a given distance.

The study at a distance of 5 mm was not further investigated, since as noted the resonance phenomenon does not occur and the temperatures remain low.

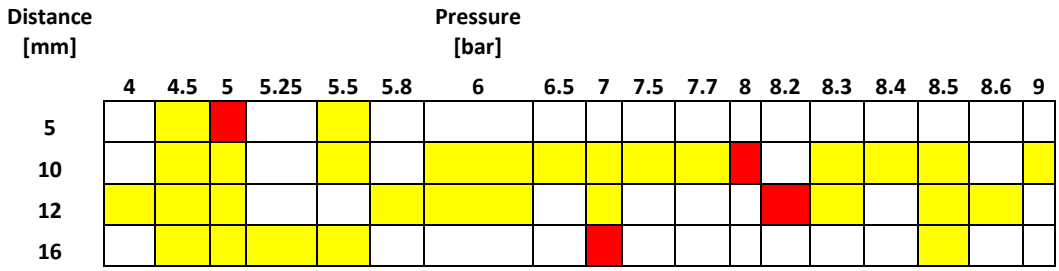

Table 4.1: Summary tests performed

For an overall view, a graph shows all the frequency peaks obtained during the tests (*Figure 4.1*). Although some changes have been made, such as the displacement of the thermocouple, the shielding of the resonator end from the cold flow coming from the nozzle and the modification of the compressed air line, all results are in line with expectations.

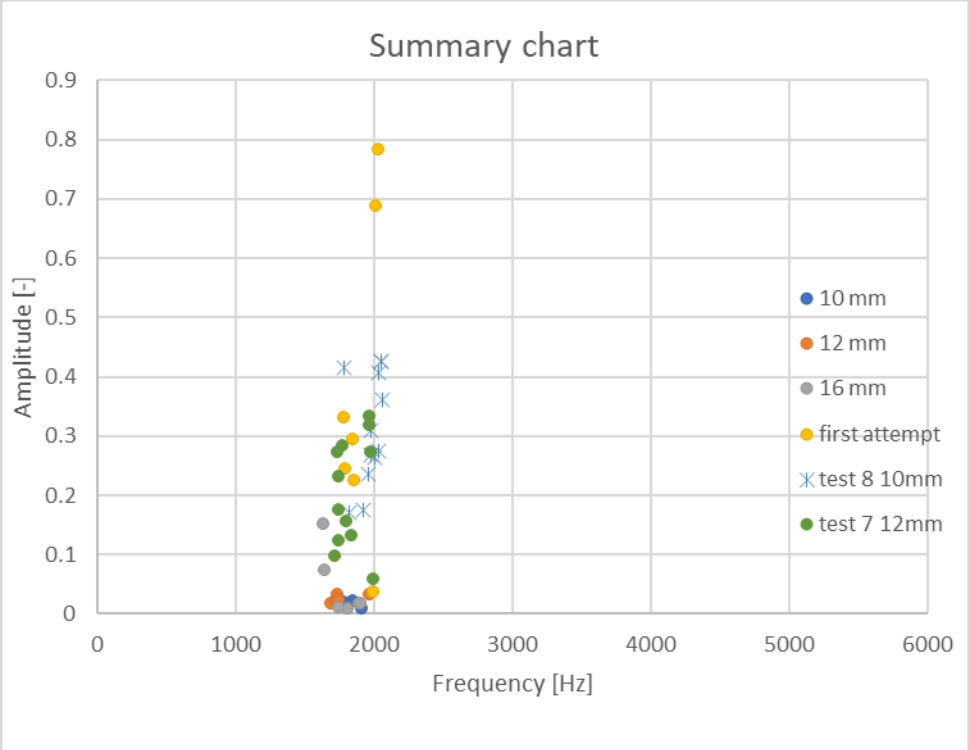

Figure 4.1: Summary graph of frequencies recorded during the three experimental campaigns

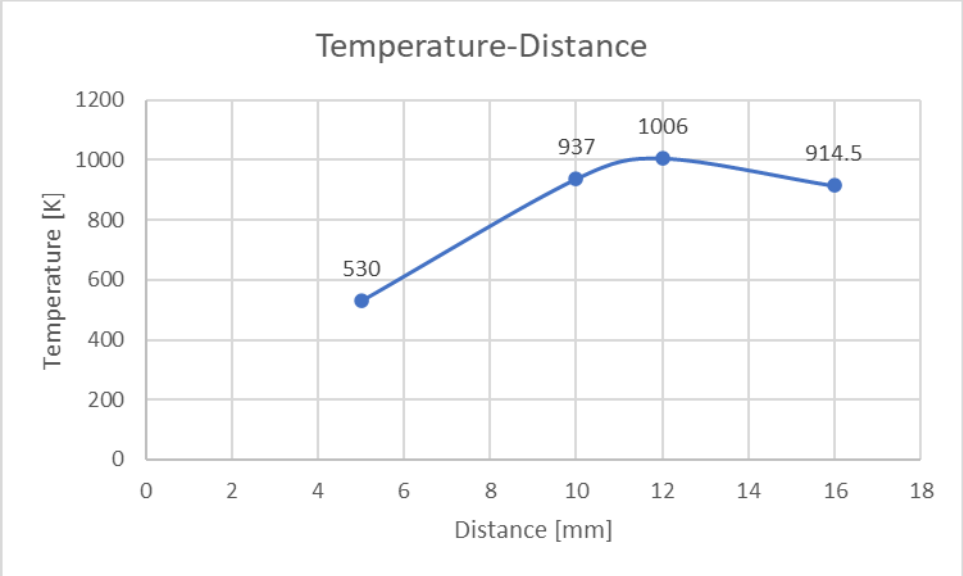

Figure 4.2: Graph of maximum temperatures as a function of the nozzle-resonator distance

By collecting the maximum values of the temperature recorded during the tests for different nozzle-resonator distances as reported in the beginning table of this final chapter, the graph of *Figure 4.2* was created.

This graph shows the optimal range at which it is possible to obtain higher temperatures with the apex around 12 mm. Moreover, this distance matches the one obtained in the 2018 study by Bauer, Pauw and Haidn.[3]

Figure 4.3 below shows the graph that compares the peak temperature reached as a function of the NPR for different values of s / d. With s / d = 1.25 the temperatures are minimum, in fact there was no resonance; s / d = 2.5 is better in terms of performance than s / d = 4 where for a greater nozzle-cavity distance the temperatures obtained are lower. However, both distances have a very flat trend for various ranges of NPR or pressures, especially for s / d = 2.5, where for NPR values between 7.5 and 10 the temperature variation is about 28 K. Finally, for s / d = 3 starting from NPR = 7 the temperatures reached are higher than the others, however the area where the maximum is present is very angular and temperatures tend to drop immediately afterwards.

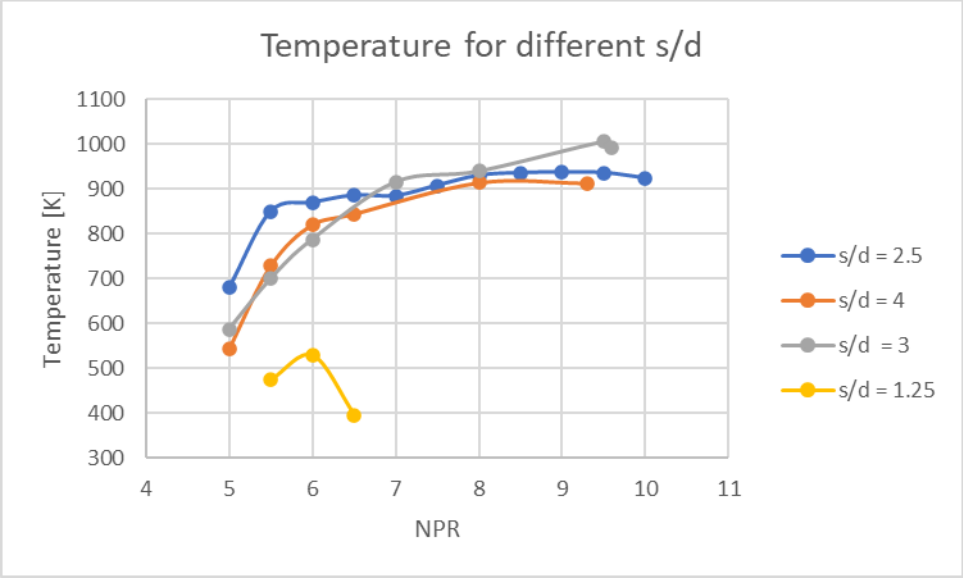

Figure 4.3: Summary graph of maximum temperatures as a function of NPR

Below is a detail of the graph with maximum temperatures recorded relative to 10 mm and 16 mm distances whose trends are very similar, however, as mentioned, the first value is more efficient.

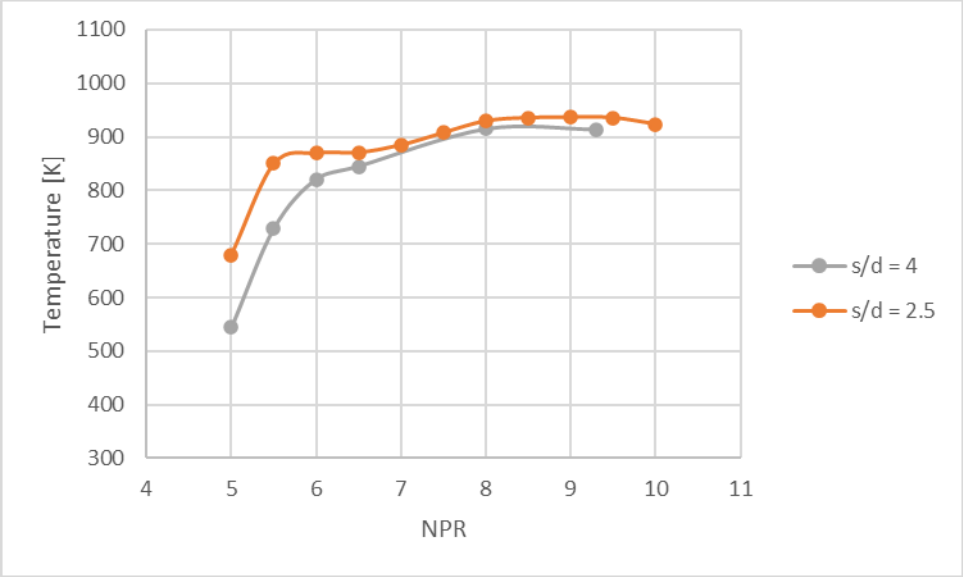

Figure 4.4: Detail of the maximum temperatures-NPR trend for 10 mm and 16 mm distances

In order to compare the greater stability of the system in terms of temperature variation for a wide range of pressures (NPR), the following graph is presented in *Figure 4.5* which shows the variation of temperatures for each nozzle-resonator distance tested, the range of NPR considered is wide and it ranges from a minimum of 7 up to 10.

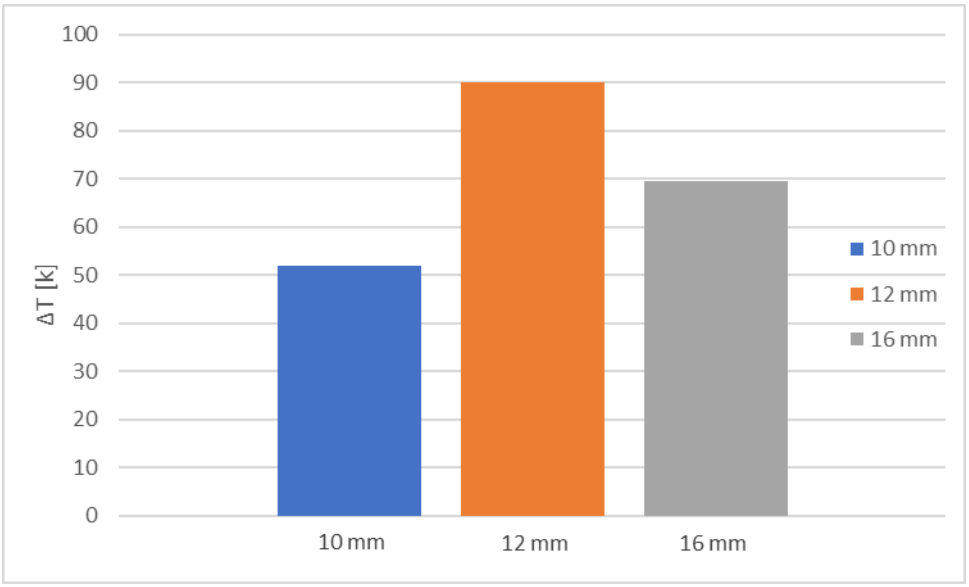

Figure 4.5: ΔT detected for a range of NPR values at different nozzle-resonator distances

As it can be seen, the distance of 10 mm is the one that has the least deviation, with ΔT of only 52 K, in fact in the previous graph the trend of s / d = 2.5 was very

constant without sudden variations. For the distance of 12 mm, although the highest temperature of 1006 K was recorded, the ΔT is greater and equal to 90 K, confirmed by the trend of the s / d curve. Finally, with an intermediate value of ΔT equal to 69.5 K, there is a distance of 16 mm corresponding to s / d = 4.

Making a comparison in terms of maximum temperature, the distance of 12 mm is the one that made it possible to reach the maximum value, while if the interest is the temperature lower oscillation, it is evident from the graph that the distance of 10 mm is to be considered optimal.

4.2 Future Developments

- **Tripping Device and New Cavity with Artificial Roughness**

Some further tests are possible in order to investigate some aspects in more details. For example the insertion of the tripping device positioned in front of the resonator inlet, as we have seen in chapter 2, has led to obtain ambiguous results; however it is possible to investigate the subject by carrying out further studies in order to evaluate the interaction between the vortex shedding and the cavity; observing which are the most influential factors, such as the distance of the disturbing element from the nozzle-outlet and its diameter.

The addition of these elements has the effect of destabilizing the flow by changing its path and behaviour as visible in some studies, in which the hydraulic analogy was used to analyze the interaction between the interferences of the disturbing element (typically wedge trip) and the pulsating flow of the resonator.[29] Various observations were collected relating the amplitude of the oscillations with the spacing between the tripping device and the cavity entrance.[28] Furthermore for higher flow velocities, the spacing, which allows to obtain the maximum resonance amplitude, increases.[28] Finally, the structure of the vortex shedding is also variable: if the disturbing element (trip rod) is placed close to the cavity, the shape of the vortex changes from asymmetrical to symmetrical.[30]

The insertion of artificial roughness inside the cavity may be of particular interest; this combination can be tested in order to evaluate its impact on the maximum temperatures obtainable. In fact, in the final stages of this study, a particular shape of the same cavity was developed with the addition of internal "obstacles" whose purpose is to destabilize the flow. In fact, in the traditional cavity, as seen in the previous chapters, part of the gas remains trapped inside, undergoing cyclical expansions and compressions leading to an increase in temperature because of

the irreversible phenomena which take place in the cavity; with the addition of further roughness, this effect should be accentuated. For the dimensioning of the obstacles, the study by Conte, Ferrero and Pastrone on the numerical simulation of the flow field in a resonant igniter was initially considered.[27]

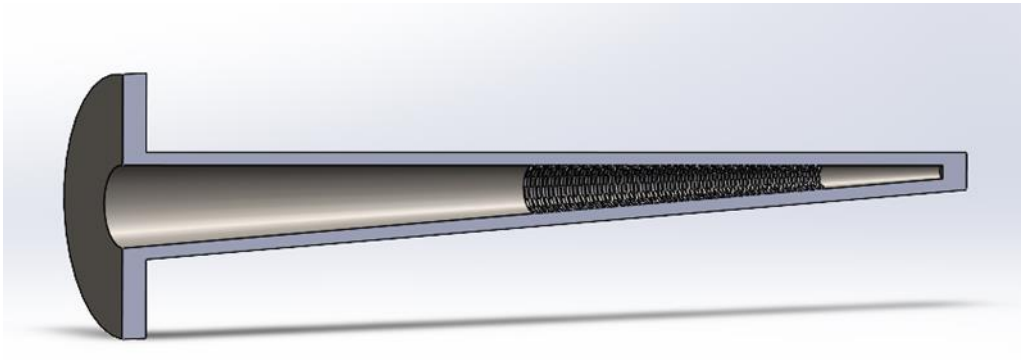

Figure 4.6: Drawing made with Solidworks® of the conical cavity with the addition of artificial roughness in the second half of it

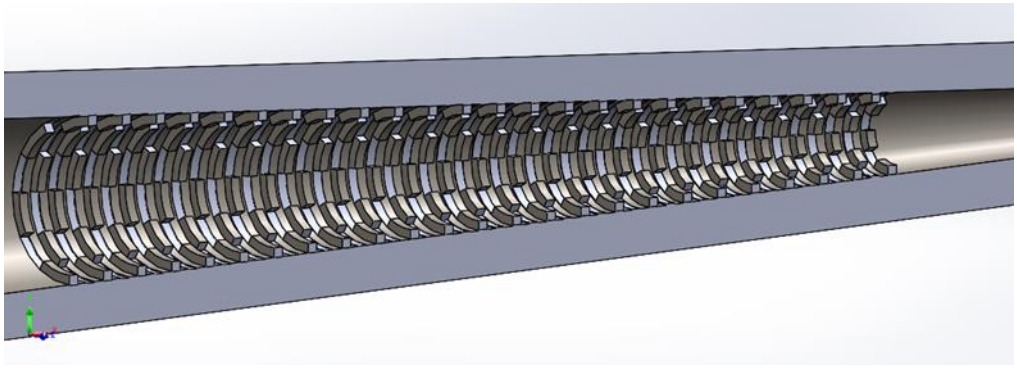

Figure 4.7: Detail of the same cavity where the inserted obstacles are visible

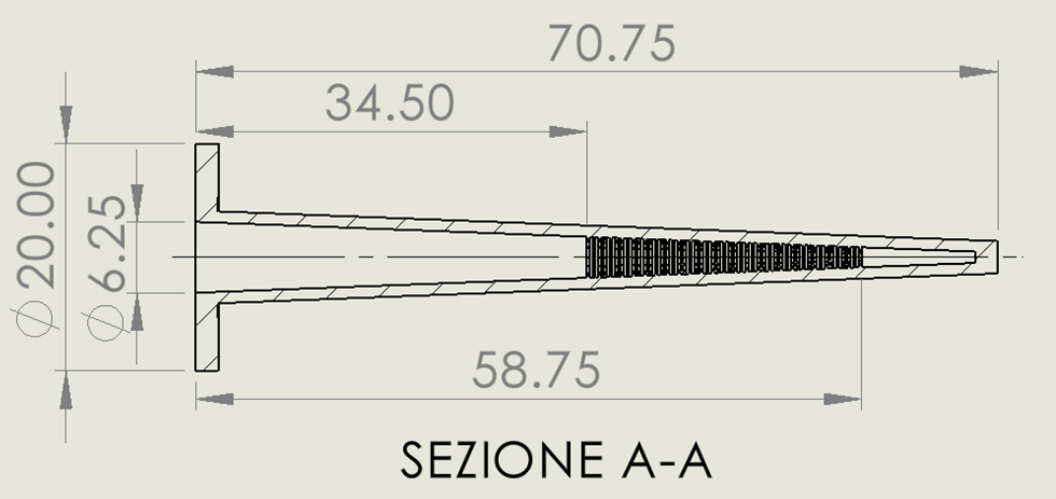

Figure 4.8: Drawing with dimensions of the conical-rough cavity

- **Cavity with an Exponential Shape**

The shape of this cavity is inspired by the exponential horn used in acoustics. In fact, the interest in this particular pattern emerged around the 20s; as is well known, this shape was used in the musical field, think for example of the trumpets.[25] There are many forms of horn including pipe, parabolic, conical, hyperbolic and exponential, the latter shape is the one of our interest.[26] The sound emitted at the root of the cavity is characterized by high pressure and low speed vibrations; the variation in diameter allows it to be amplified to obtain sound waves characterized by low pressure and high speed in the final section of greater diameter.[25] Its purpose is to increase the output by concentrating the sound emission in a certain direction.[26]

However, the thermal effects related to this form are still unknown, therefore of particular interest may be the comparison of the maximum temperatures reached by this exponential cavity with the conical shape used for carrying out the previous test in chapter 3.

Below, in *Figures 4.9* and *4.10*, are shown the 3D drawing and the dimensioned one of the exponential cavity for the resonator.

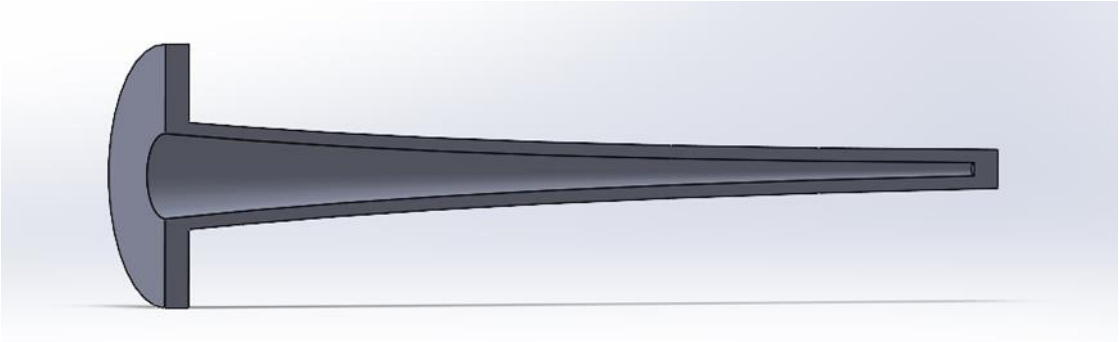

Figure 4.9: Exponential cavity, section view

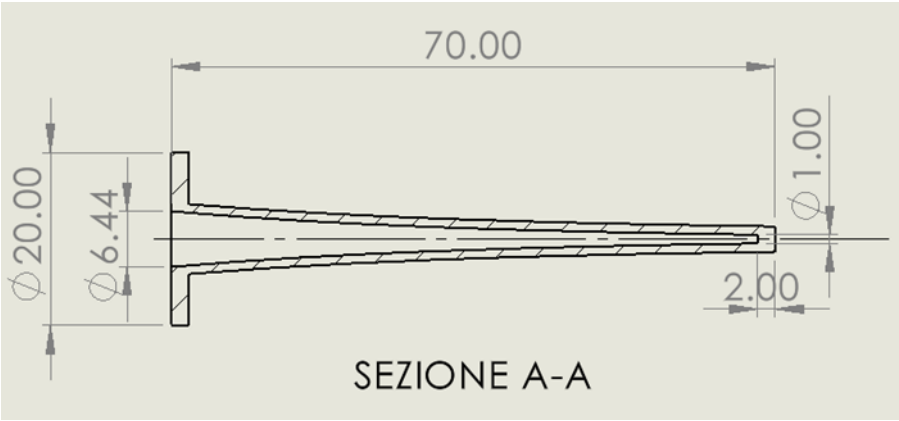

Figure 4.10: Dimensioned drawing of the exponential cavity

Bibliography

[1] B.Phillips, A.J.Pavli. “Resonance Tube Ignition Of Hydrogen-Oxygen Mixtures”. Nasa Techical Note TN D-6354, 1971.

[2] Sarohia, Back, Roschke e Pathasarathy. “An Experimental Investigation of Fluid Flow and Heating in Various Resonance Tube Modes”. NASA-CR-148760, 1976.

[3] Bauer, Pauw, Haidn. “Numerical and Experimental Investigation on Resonance Ignition”. Istitute for Flight Propulsion, Technische Universitat Munchen.

[4] A.K.Gupta. “Numerical and Experimental Investigation of Resonance Igniter and its Optimisation Using Genetic Algorithm”. AIAA Propulsion and Energy Forum, 2020.

[5] Lungu, Bauer, Haidn. “Design aspects and characterisation of a resonance igniter for oxygen/methane in-orbit propulsion systems”. Technische Universitat Munchen, Institute for Turbomachinery and Flight Propulsion, 8th European Conference for Aeronautics and Space Sciences (EUCASS), 2019.

[6] V.Sarohia, E.J.Roschke, S.P.Pathasarathy, L.H.Back. “An Experimental Investigation of Fluid Flow and Heating in Various Resonance Tube Modes”. JPL, technical Memorandum 33-780, 1976.

[7] J.Hartmann. “On a New Method for the Generation of Sound Waves”. Physical Review, Vol.20 No. 6, 1922.

[8] E.Brocher, J.P.Ardissone. “Heating characteristics of a new type of Hartmann-Sprenger tube”. The International Journal of heat and fluid flow, Vol.4 (2), p.97-102, 1983.

[9] Li Bo, Hu Guo-hui, Zhou Zhe-wei. “Numerical simulation of flow in Hartmann resonance tube and flow in ultrasonic gas atomizer”. Applied Mathematics and Mechanics, 28(11):1415-1426, 2007.

[10] G.Raman, K.Srinivasan. “The powered resonance tube: From Hartmann’s discovery to current active flow control applications”. Progress in aerospace sciences, Vol. 45 (4), p.97-123, 2009.

[11] B.Afzali, H.Karimi. “Numerical Investigation on thermo-acoustic effects and flow characteristics in semi-conical Hartmann-Sprenger resonance tube”. Proceedings of the Institution of Mechanical Engineers. Part G, Journal of aerospace engineering, 2017-12, Vol.231 (14), p.2706-2722, 2017.

[12] S.Murugappan, E.Gutmark. “Parametric study of the Hartmann-Sprenger tube”. Experiments in Fluids, Vol.38 (6), p.813-823, 2005.

[13] A.Goldshtein, A.Alexeev, C.Gutfinger. “Resonance oscillations with thermal effects of an inviscid gas in a closed tube”. Journal of fluid mechanics, Vol.518, p.1-34, 2004.

[14] B.Afzali, H.Karimi. “Effect of pipe geometry and material properties on flow characteristics and thermal performance of a conical Hartmann-Sprenger tube”. Journal of the Brazilian Society of Mechanical Sciences and Engineering, 2017-11, Vol.39 (11), p.4489-4501, 2017.

[15]M.Kawahashi, R.Bobone, E.Brocher. “Oscillation modes in single-step Hartmann-Sprenger tubes”. The journal of the Acoustical Society of America, Vol.75 (3), p.780-784, 1984.
[16]P.V. Kadaba, V.L.Bondarenko, A.M.Arkharov. “Thermal characteristics of a Hartmann-Sprenger tube”. International journal of refrigeration, Vol.13 (5), p.309-316, 1990.
[17]R.A.Marchan. “Small-Scale Supersonic Combustion Chamber with a Gas-Dynamic Ignition System”. Combustion Science and Technology, 183:11, 1236-1265, 2011.
[18]https://www.cnet.com/products/logitech-dialog-320-microphone-series/ Microfono
[19]H.Sprenger. “Uber thermische Effekte in Resonanzrohren”. Zurich, 1954.
[20]T.Vrebalovich. “Resonance tubes in a supersonic flow field”. JPL, Technical report No. 32-378, 1962.
[21]E.Brocher, C.Maresca. “Etude des phenomenes thermiques dans un tube de Hartmann-Sprenger”. International journal of heat and mass transfer, Vol.16 (3), p.529-538, 1973.
[22]https://en.wikipedia.org/wiki/Thermocouple
[23]www.thermometricscorp.com/thertypk.html Type K thermocouple
[24]https://productz.com/en/logitech-dialog-320/p/axLNR microfono Logitech® Dialog 320
[25]https://blog.sciencemuseum.org.uk/ in search of perfect sound. 2014.
[26]Bjorn Kolbrek. “Horn Theory: An Introduction”. Audioxpress
[27]A. Conte, A. Ferrero, D.Pastrone. “Numerical investigation for performance prediction of gas dynamic resonant igniters”. Advances in Aircraft and Spacecraft Science, Vol. 7, No. 5, p. 425-440, 2020.
[28]K. Hourigan, M.C.Thompson, E.Brocher, A.Andrianantoandro. “Coupling of Vortex Shedding with the Fundamental Resonant Mode of a Resonator Tube”. Noise Control Engineering Journal, Vol.41, No.2, 1993.
[29]M. Kawahashi, E. Brocher, P. Collini. “Coupling of vortex shedding with a cavity”. Fluid dynamics research, Vol.3 (1), p. 369-375, 1988.
[30]M.C. Thompson, K. Hourigan, M.C. Welsh, E. Brocher. “Acoustic Sources in a Tripped Flow past a Resonator Tube”. AIAA Journal, Vol.30, No.6, 1992.

Acknowledgements

I would like to thank the laboratory staff of the Aerospace Engineering Department Ing. Grivet and Ing. Cannata for the availability provided during the tests.

My thanks go also to Ing. Giulio Marchese and Prof.ssa Sara Biamino of the Department of Applied Science and Technology for the construction of the resonator, object of this study.